Physics 129 LECTURE 17 March 11, 2014

Galaxies, Nucleosynthesis, and Light

- Galaxy Formation Theory
- Feedback Solves Angular Momentum Problems
- Eris - Successful Simulation of Milky Way-type Galaxy
- *Sunrise* Makes Realistic Images from Simulations
- Semi-Analytic Models (SAMs) Predict Galaxy Population Evolution Based on Cosmological Merger Trees
- Production of Chemical Elements by Stars,Supernovae, and Neutron Star Mergers
- Measuring the Rate of Galaxy Mergers
- Blue (star forming) and Red (quenched) Galaxies
- Measuring the Extragalactic Background Light Using Gamma Ray Astronomy

Galaxy Formation Theory

Primordial fluctuations grow due to inflation.

Baryons trace the DM distribution in scales larger than the Jeans length

e.g. Rees & Ostriker 1977, White & Rees 1978, White & Frenk 1991, Kauffmann et al. 1993, Cole et al. 1994, Somerville & Primack 1999, Sommerville et al. 1998, Birnboim & Dekel 2003

Dark matter undergoes gravitational collapse (no pressure support) and generates at cosmic web

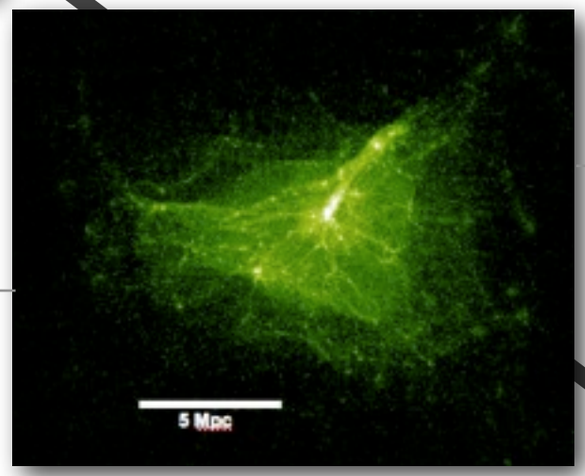

Governato et al. 2007

The angular momentum of the halo is acquired through cosmological torques

Question: How is the angular momentum of the stars related to that of the dark matter? Only ≲ 20% of the baryons in galaxy halos become stars.

Baryonic material accretes onto the dark matter potentials via hot/cold accretion.

Supersonic gas accreting at $T < T_{vir}$ is shocked near R_{vir} when $t_{cool} > t_{dyn}$ and at smaller radii if $t_{cool} < t_{dyn}$

Bertshinger 1985, Book & Benson 2010

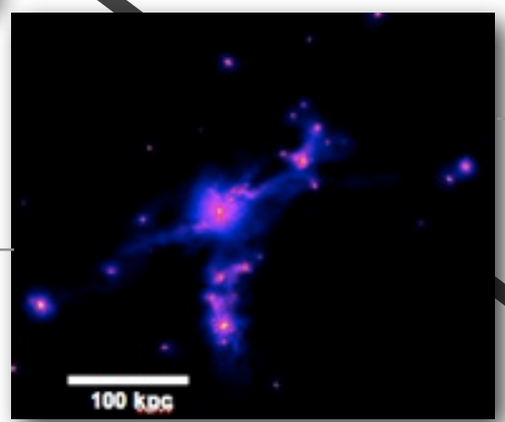

Governato et al. 2007

In halos of mass $M < 10^{11}\ M_{\odot}$ (pristine gas) shocks cannot form near R_{vir} and cold gas can accrete through filaments

Birnboim & Dekel 2003

Dissipative processes *cool* the shocked gas: atomic, Compton, molecular hydrogen cooling

Other processes *heat* gas: photo-heating, feedback, preheating, thermal conduction

Conservation of angular momentum during collapse produces disks. Feedback removes low angular momentum material.

Cosmological Simulations

Astronomical observations represent snapshots of moments in time. It is the role of astrophysical theory to produce movies -- both metaphorical and actual -- that link these snapshots together into a coherent physical theory.

Cosmological dark matter simulations show large scale structure, growth of structure, and dark matter halo properties

Hydrodynamic galaxy formation simulations: evolution of galaxies, formation of galactic spheroids via mergers, galaxy images in all wavebands including stellar evolution and dust

The Angular Momentum Catastrophe

In practice it is not trivial to form galaxies with massive, extended disks and small spheroids. The angular momentum content of the disk determines its final structure. None of the 2012 Aquila low-resolution galaxy simulations had realistic disks.

fraction of stars with given angular momentum

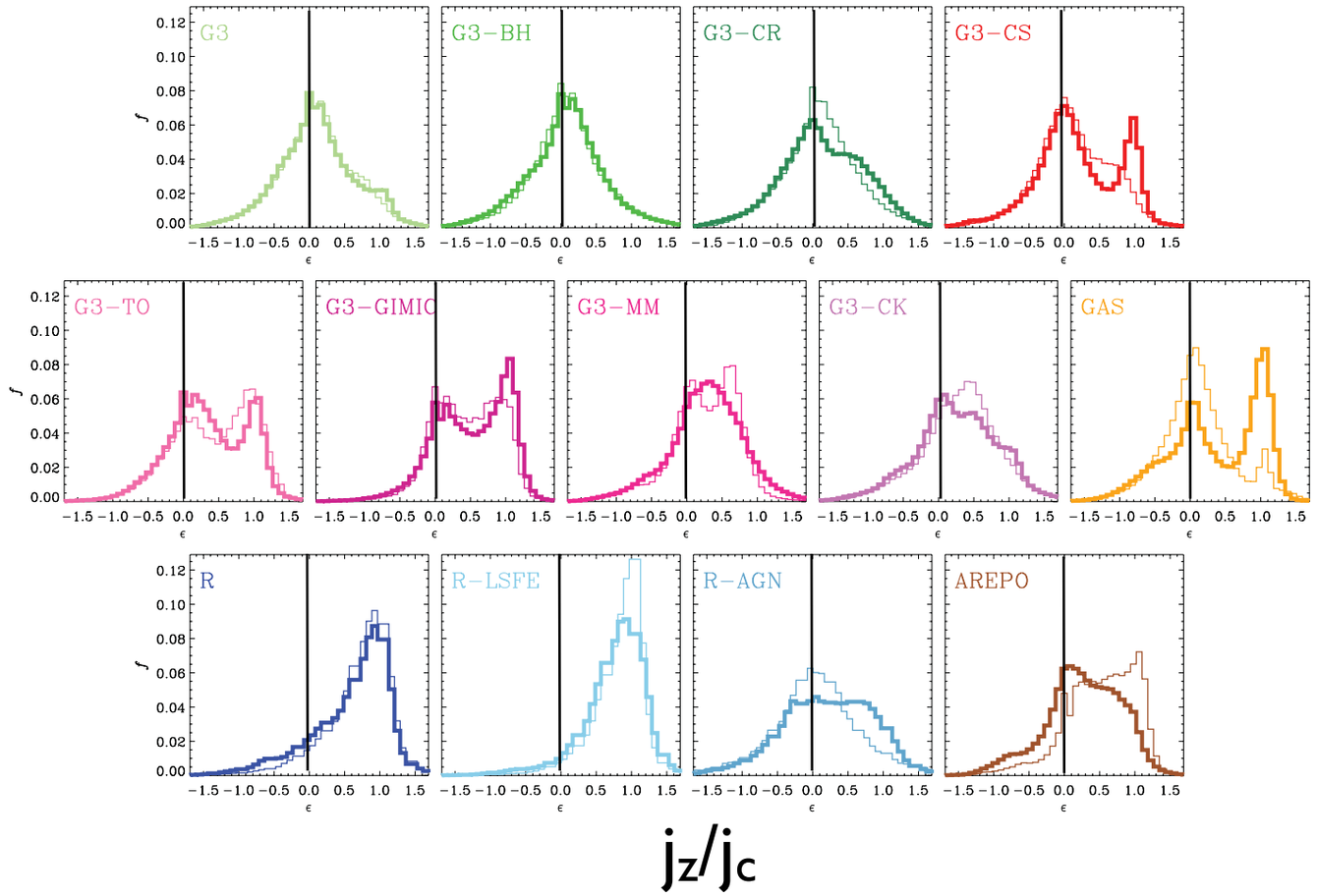

≠

Scannapieco et al., Aquila Galaxy Simulation Comparison, 2012

The Angular Momentum ~~Catastrophe~~

Eris, the first high-resolution simulation of formation of a ~10^{12} $M_\odot$ galaxy, produced a realistic spiral galaxy. Adequate resolution and physically realistic feedback appear to be sufficient.

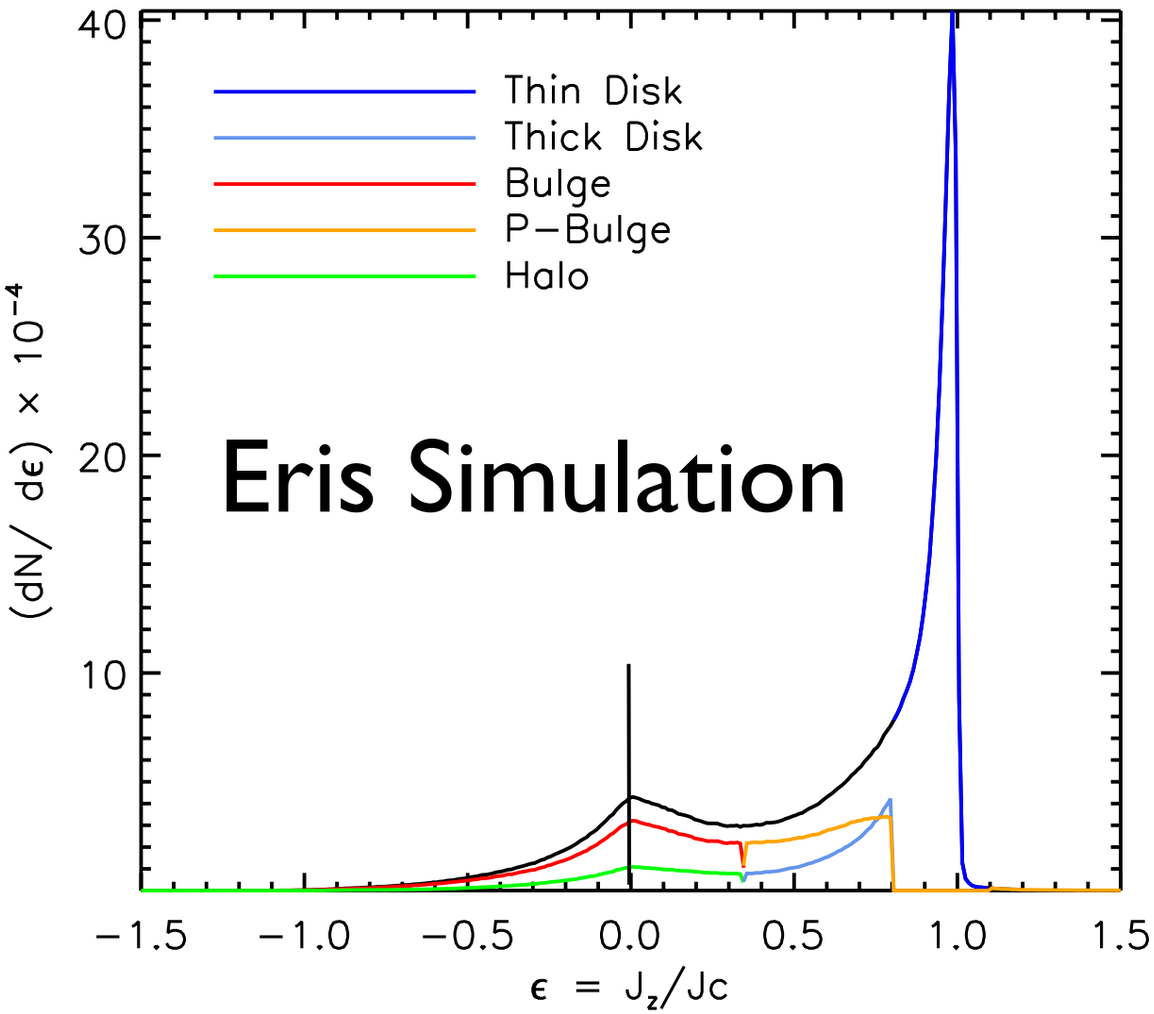

=

Guedes, Callegari, Madau, Mayer 2011 ApJ

z=90.73

Eris

Simulation
Guedes et al.

No Angular Momentum Problem in the Eris Simulation

Simulations tend to produce too many stars at the center, which translates into steeply rising rotation curves.

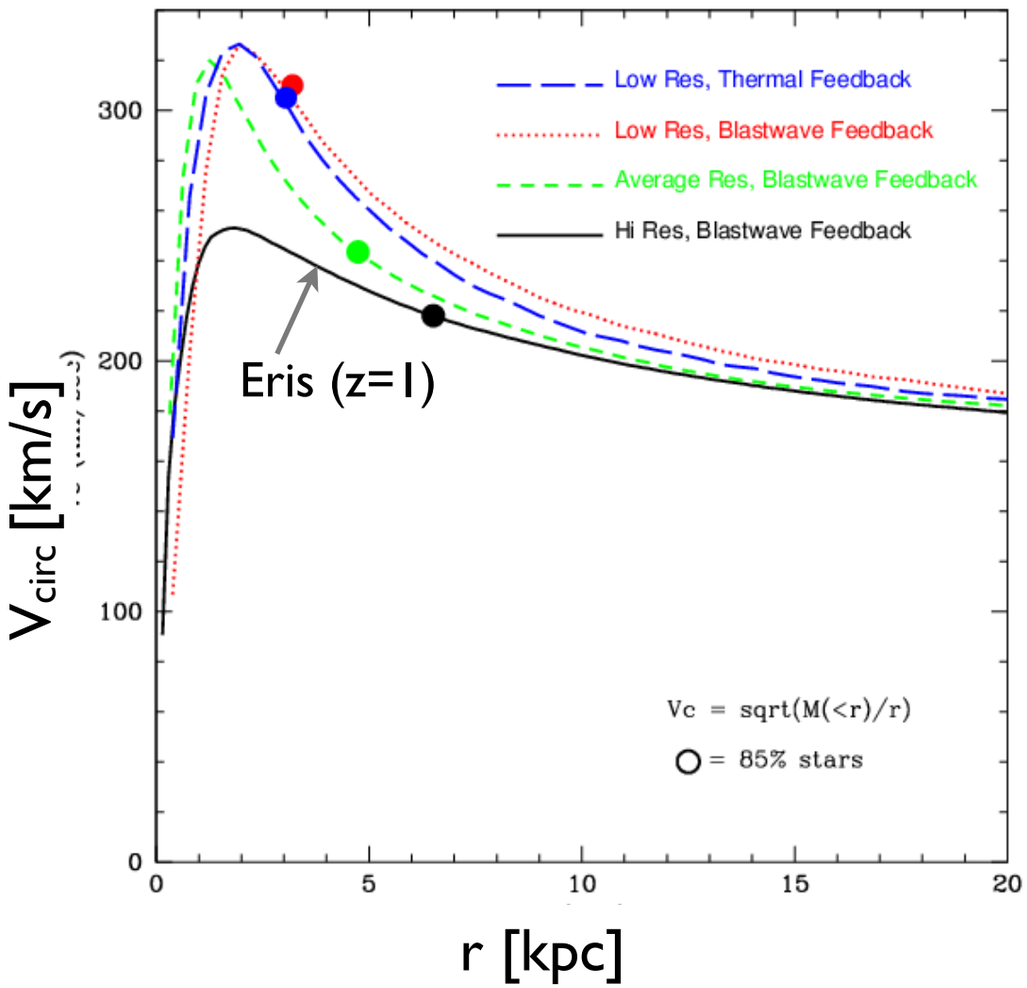

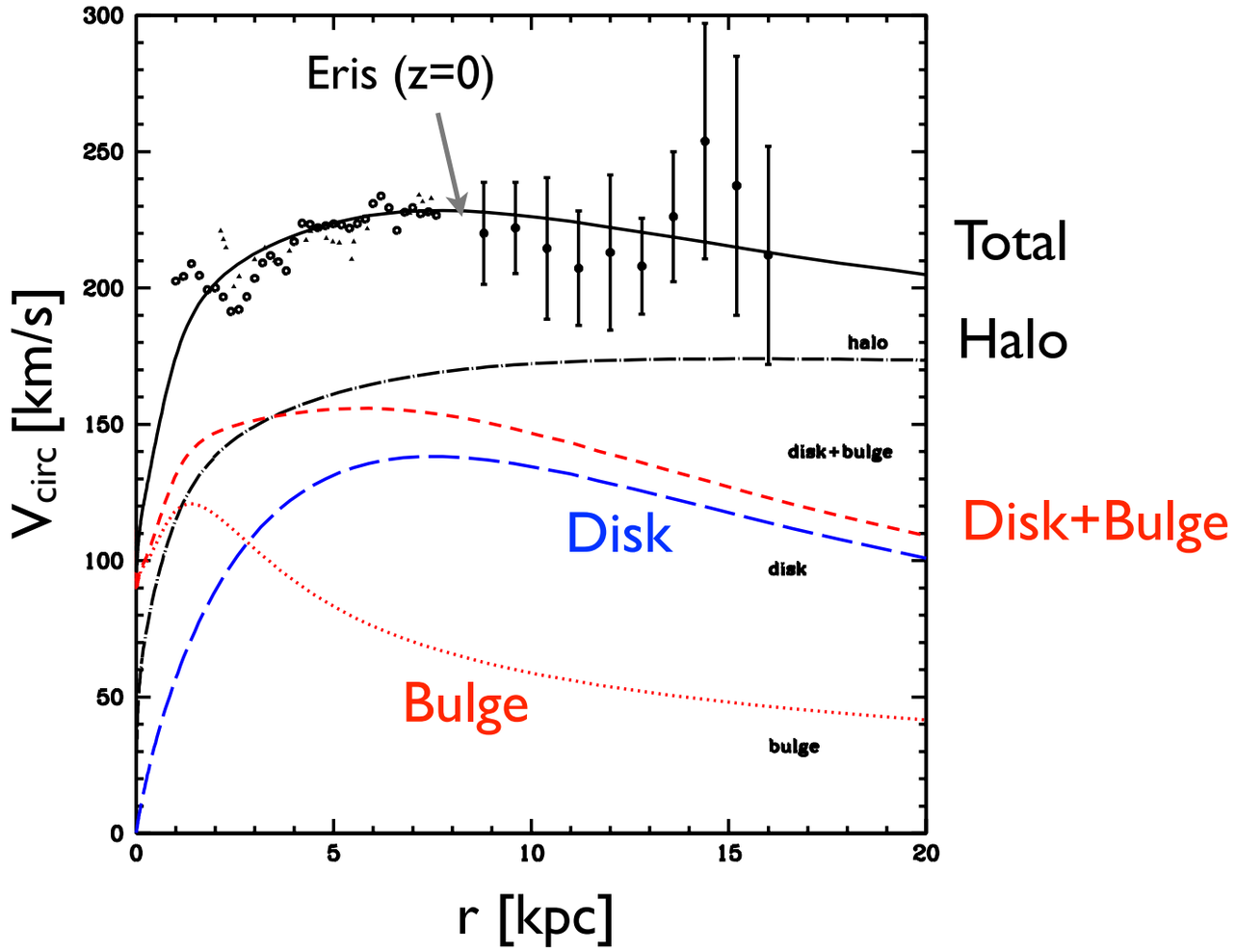

Solution:

* Mimic star formation as occurs in real galaxies, i.e. localized, on high-density peaks only.
* Feedback from SN becomes more efficient in removing gas from high-density regions.

These outflows remove preferentially low angular momentum material, suppressing the formation of large bulges.

Guedes, Callegari, Madau, Mayer 2011 ApJ

Structural Properties: Eris Bulge-to-Disk Ratio

Eris Sunrise Images: Edge On Face On

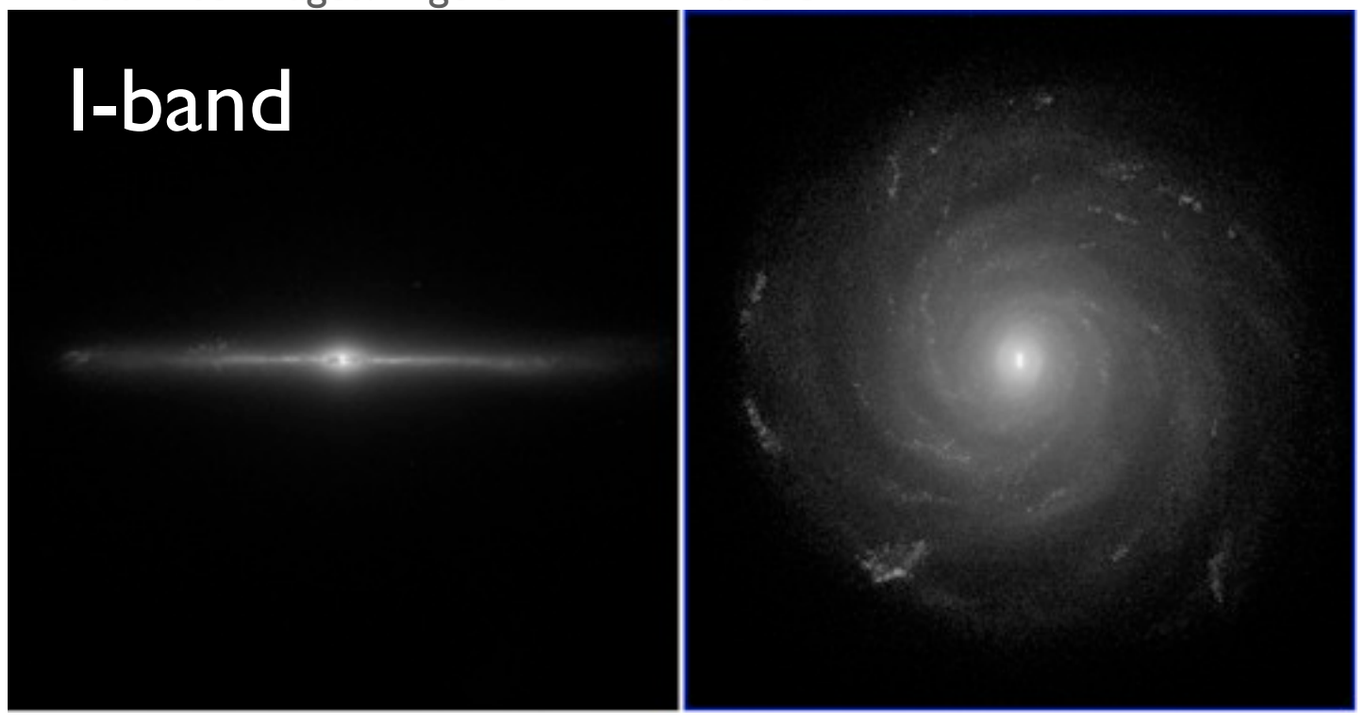

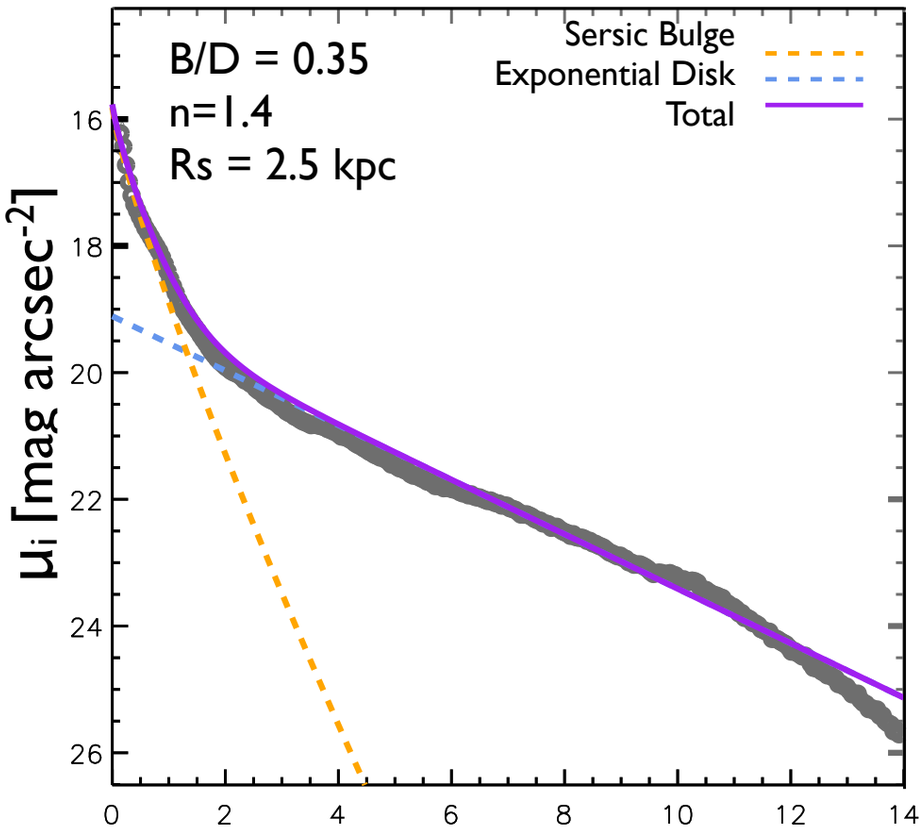

Ganda et al. 2006, 2009

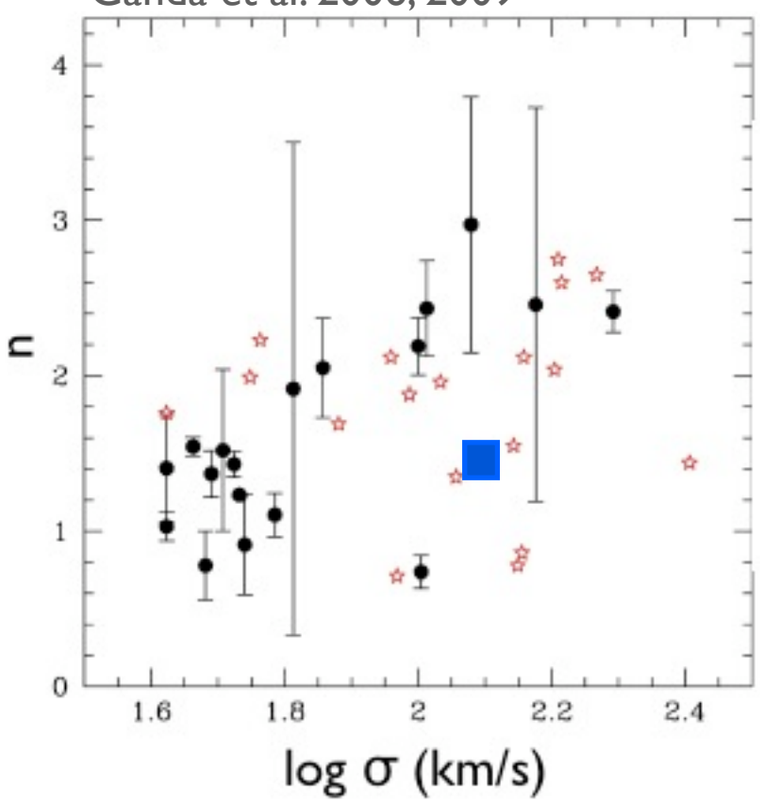

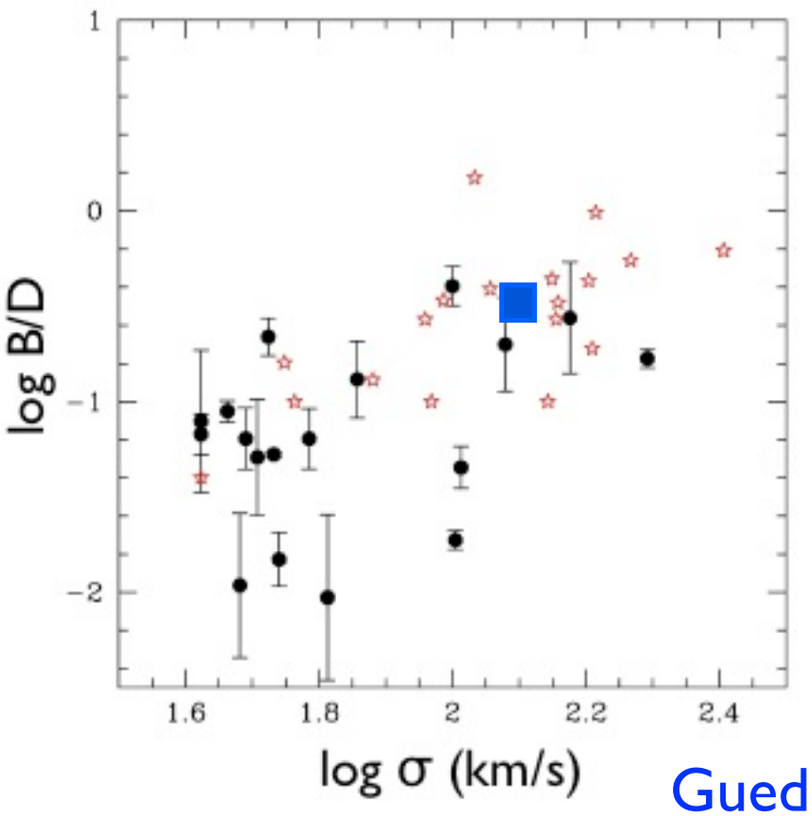

Photometric decomposition in i-band using Galfit (Peng et al. 2002)

- ● Late-type spirals
- ☆ Early-type spirals
- ■ Eris

Guedes, Callegari, Madau, Mayer 2011 ApJ

Sunrise Radiative Transfer Code

Patrik Jonsson
& Joel Primack

For every simulation snapshot:

- Evolving stellar spectra calculation
- Adaptive grid construction
- Monte Carlo radiative transfer
- “Polychromatic” rays save 100x CPU time
- Graphic Processor Units give 10x speedup

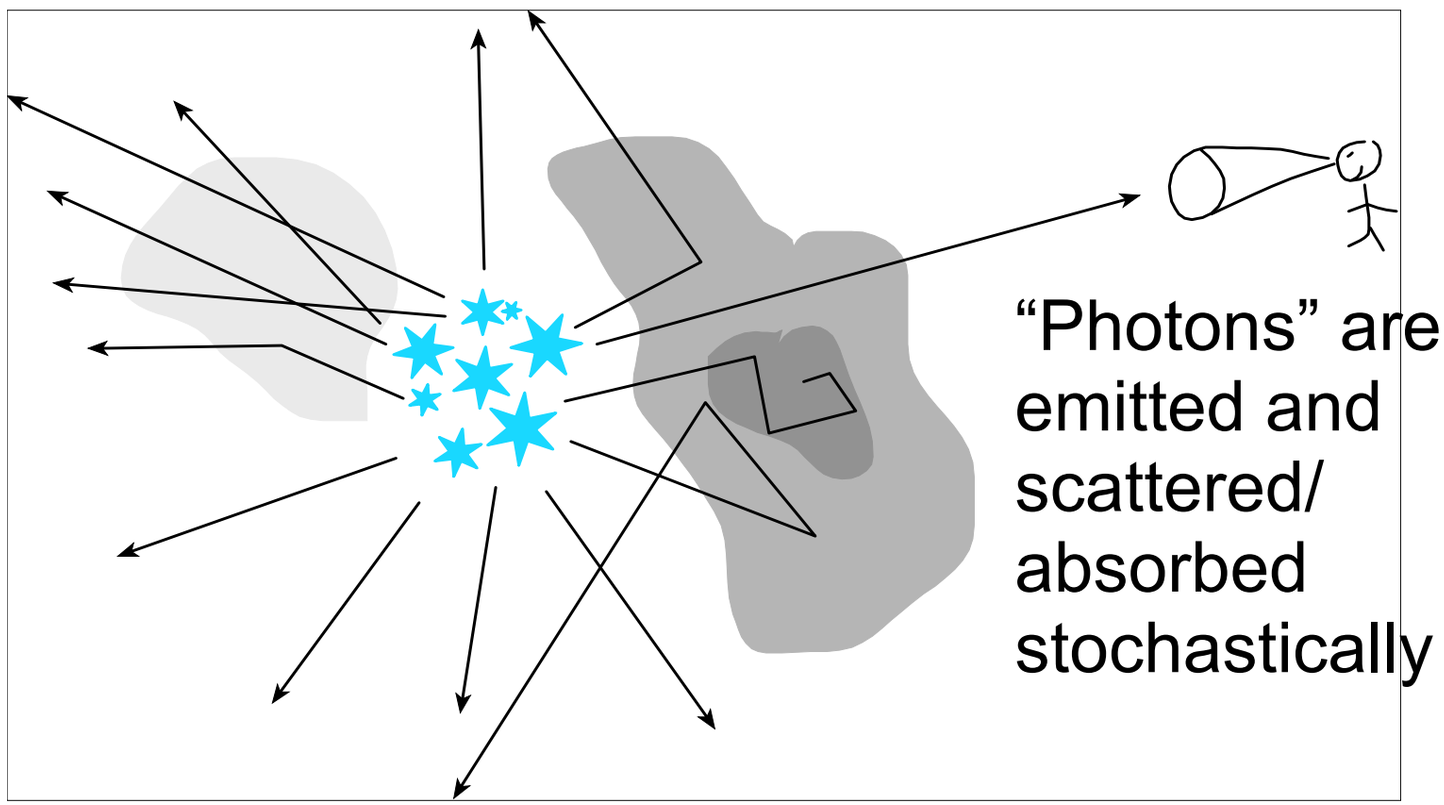

Sunrise Spectral Energy Distribution

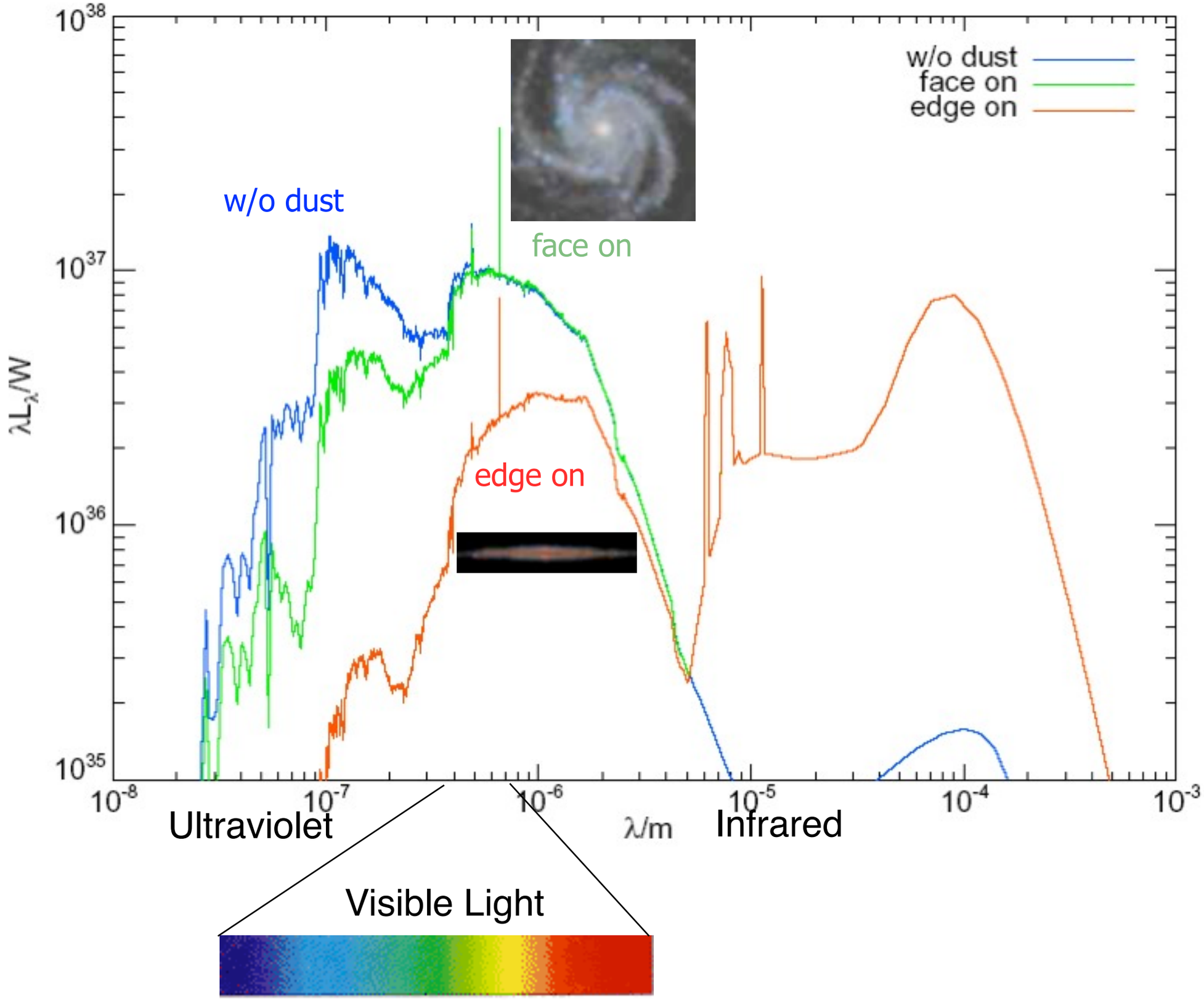

What's the effect of including dust?

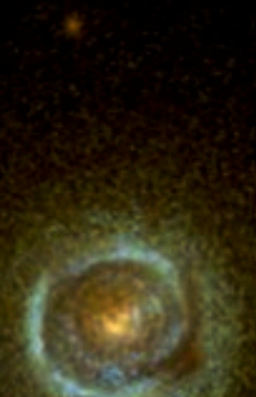

with
dust

Dramatic effects on
-Appearance
-Half-mass radii (bigger with dust)
-Sersic index (lower with dust)

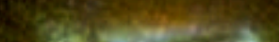

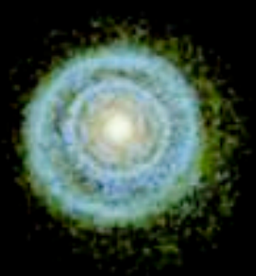

stars
only

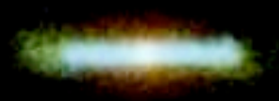

cemoody.imgur.com

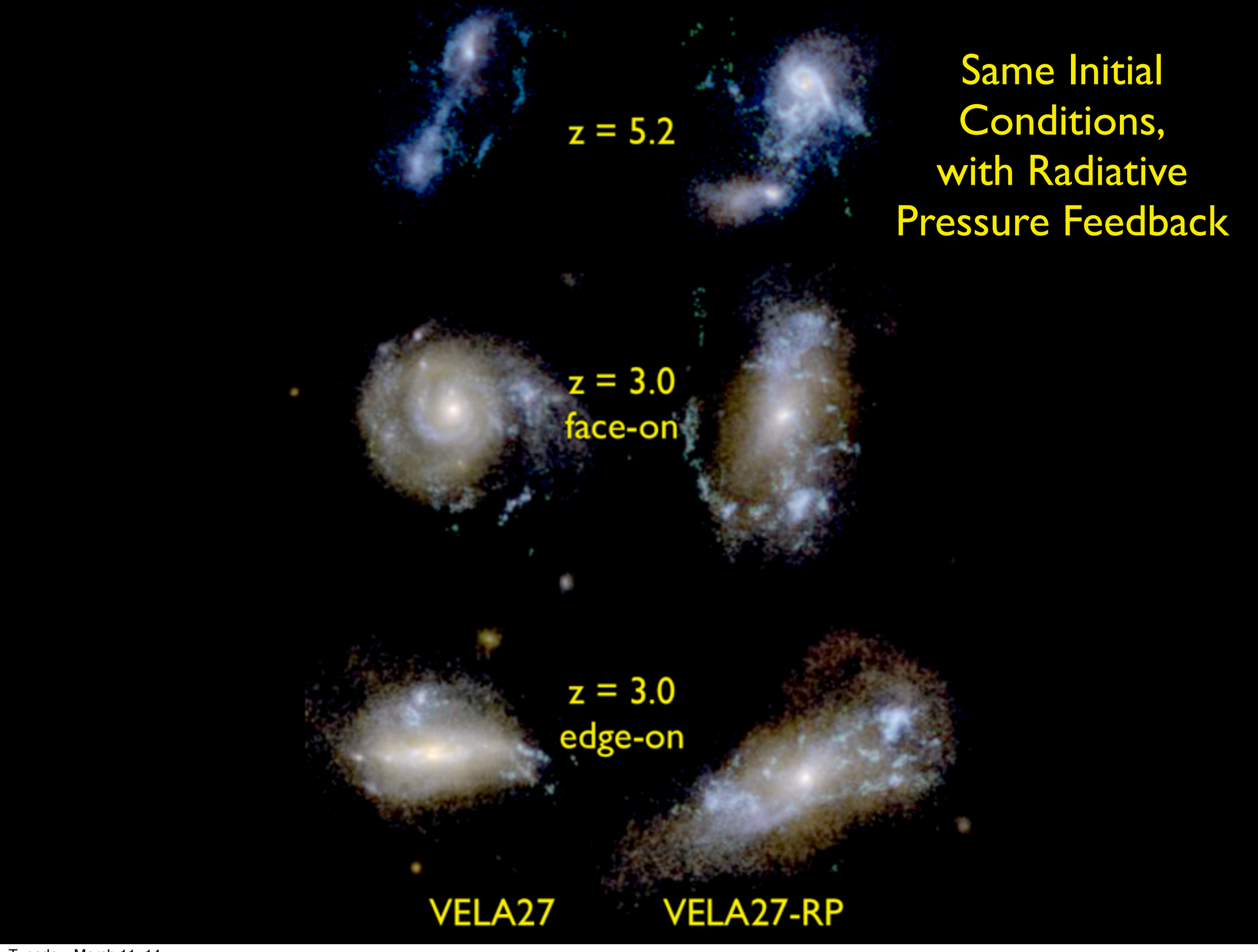

Same Initial Conditions, with Radiative Pressure Feedback

Simulated Galaxy 10 billion years ago

as it would appear nearby to our eyes

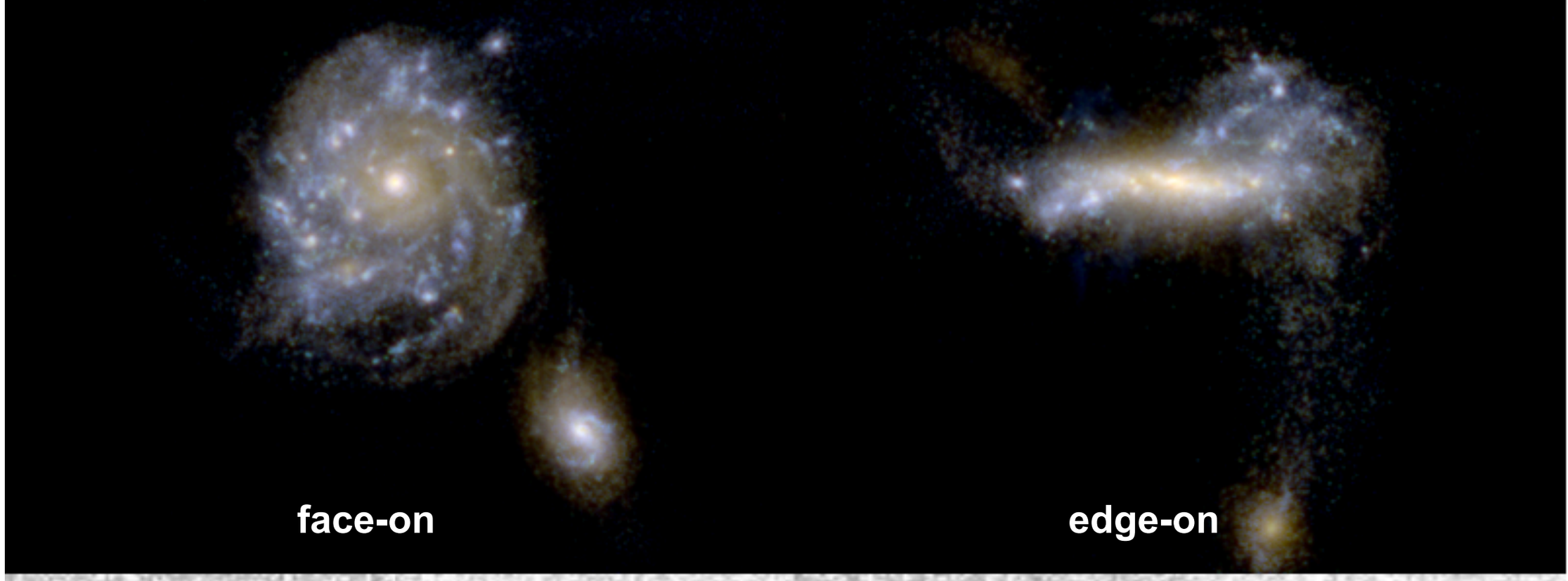

as it would appear to Hubble's ACS visual camera

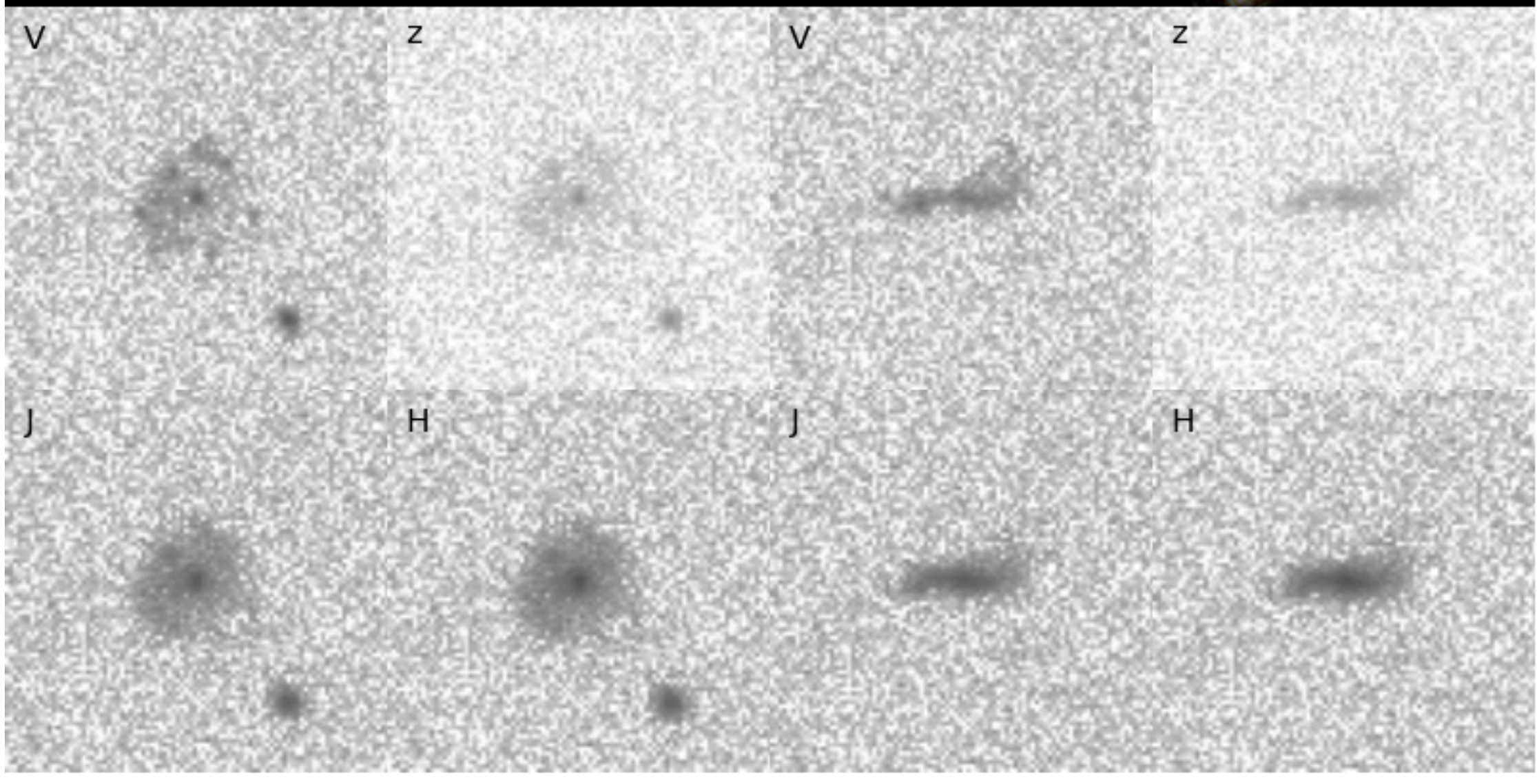

as it would appear to Hubble's WFC3 infrared camera

Our Simulations w/ Dust look a lot like galaxies from 10 billion years ago that we see with Hubble Space Telescope

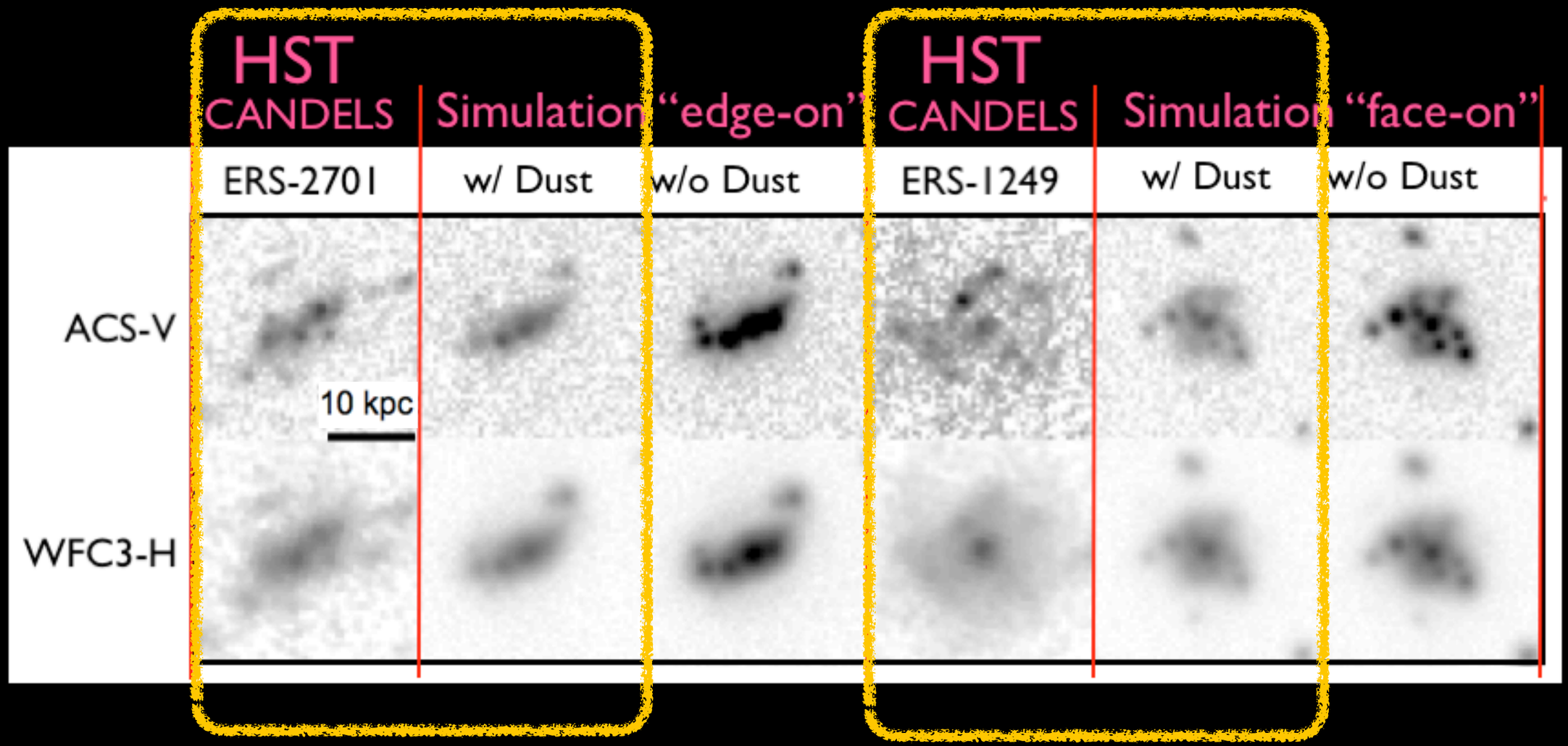

We are now systematically comparing simulated and observed galaxy images

Merger Trees

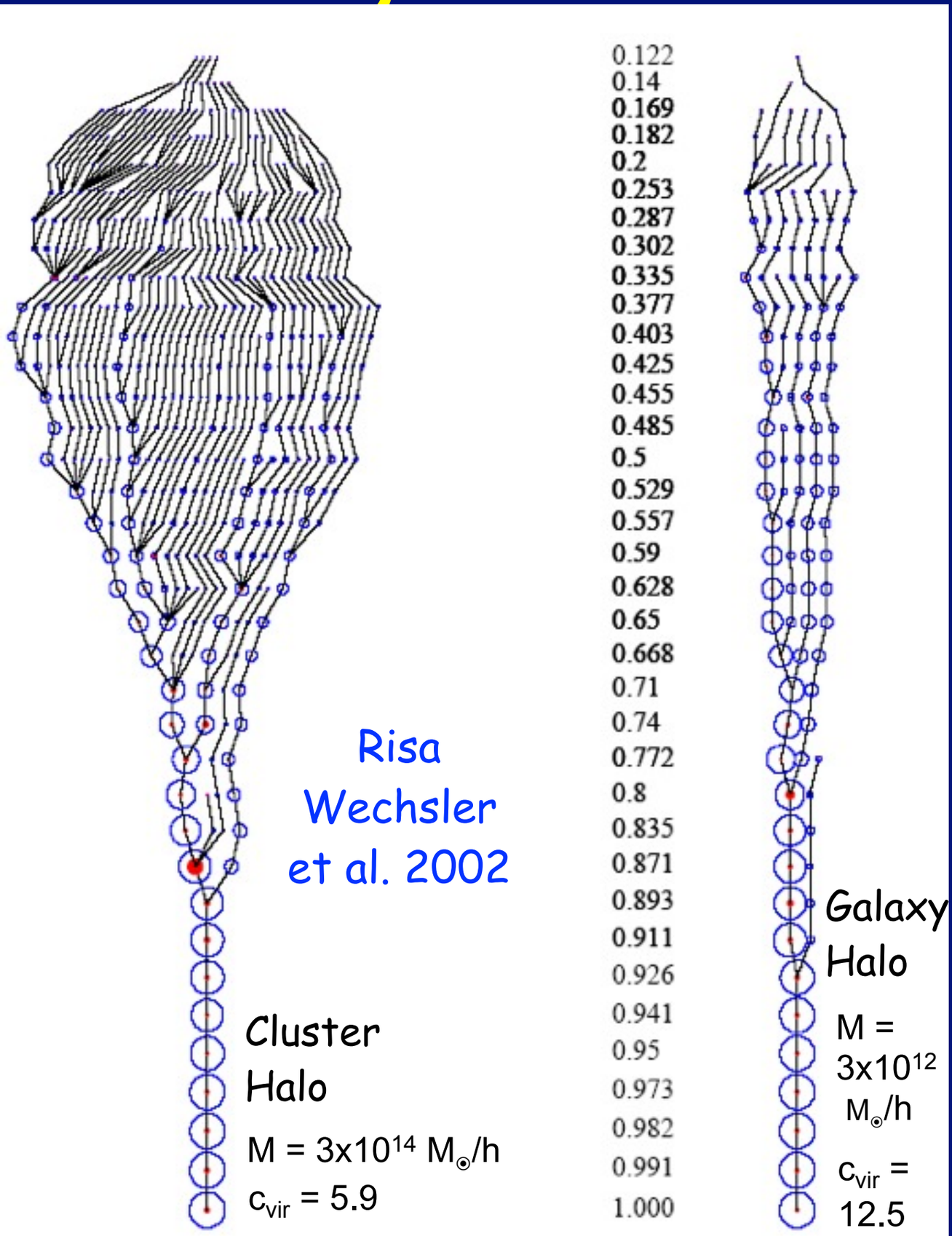

Risa Wechsler et al. 2002

Cluster Halo

$M = 3x10^{14}\ M_\odot/h$

$c_{vir} = 5.9$

Galaxy Halo

$M = 3x10^{12}\ M_\odot/h$

$c_{vir} = 12.5$

Based on our ART simulations, in her PhD research with me Risa Wechsler created the first structural merger trees tracing the merging history of thousands of halos with structural information on their higher-redshift progenitors, including their radial profiles and spins. This led to the discovery that a halo's merging history can be characterized by a single parameter a_c which describes the scale factor at which the halo's mass accretion slows, and that this parameter correlates very well with the halo concentration, thus showing that the distribution of dark matter halo concentrations reflects mostly the distribution of their mass accretion rates. We found that the radius of the inner part of the halo, where the density profile is roughly 1/r, is established during the early, rapid-accretion phase of halo growth (a result subsequently confirmed and extended by other groups, e.g., Zhao et al. 2003, Reed et al. 2004).

Galaxy Correlation Functions

Points with Errors are SDSS data

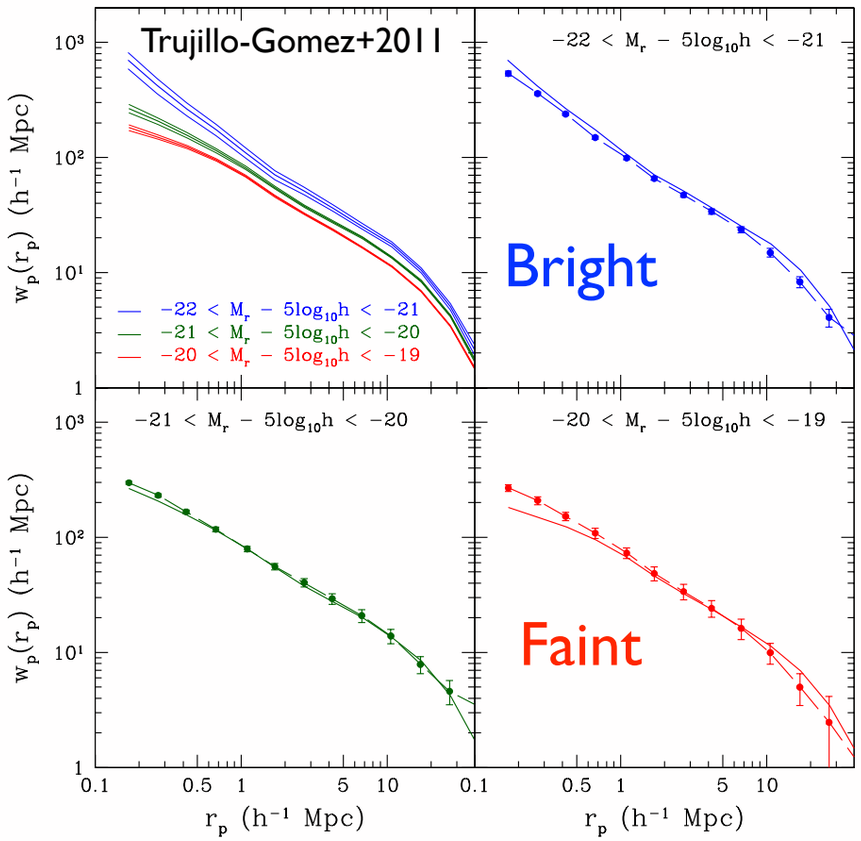

Fraction of Milky Way Mass Halos Hosting SMC/LMC Mass Satellites

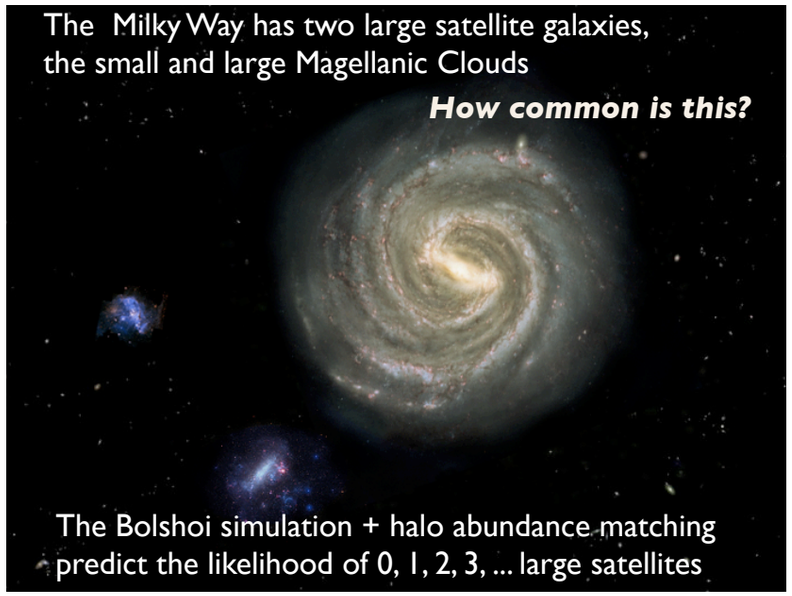

Statistics of MW bright satellites:

Sloan Digital Sky Survey data vs. Bolshoi simulation

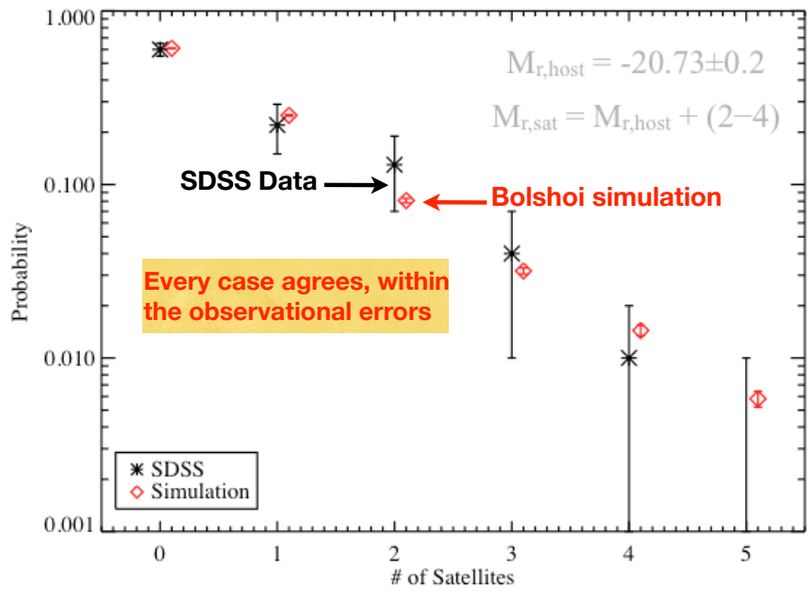

Galaxy Correlation Functions

Using Halo Age Matching

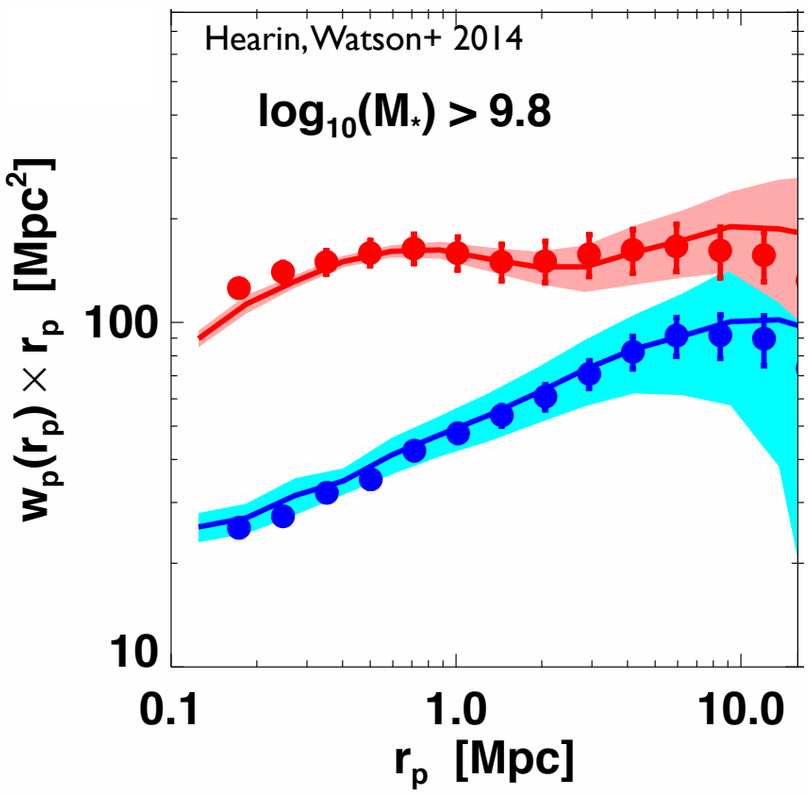

Star Formation Most Efficient at ~10^{12} $M_\odot$

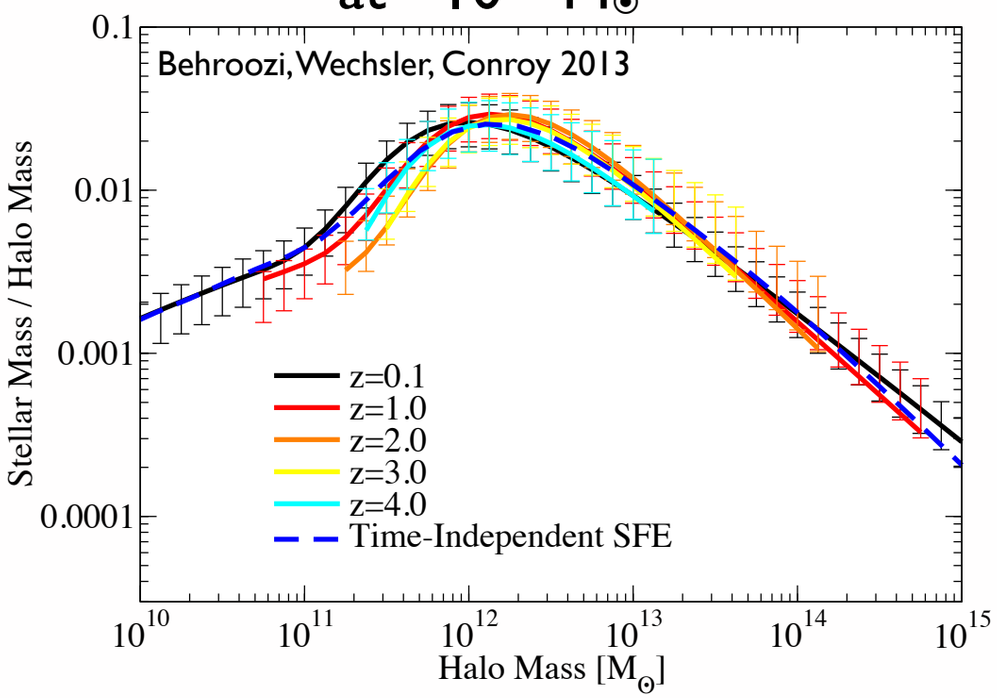

Galaxy Formation via SemiAnalytic Models

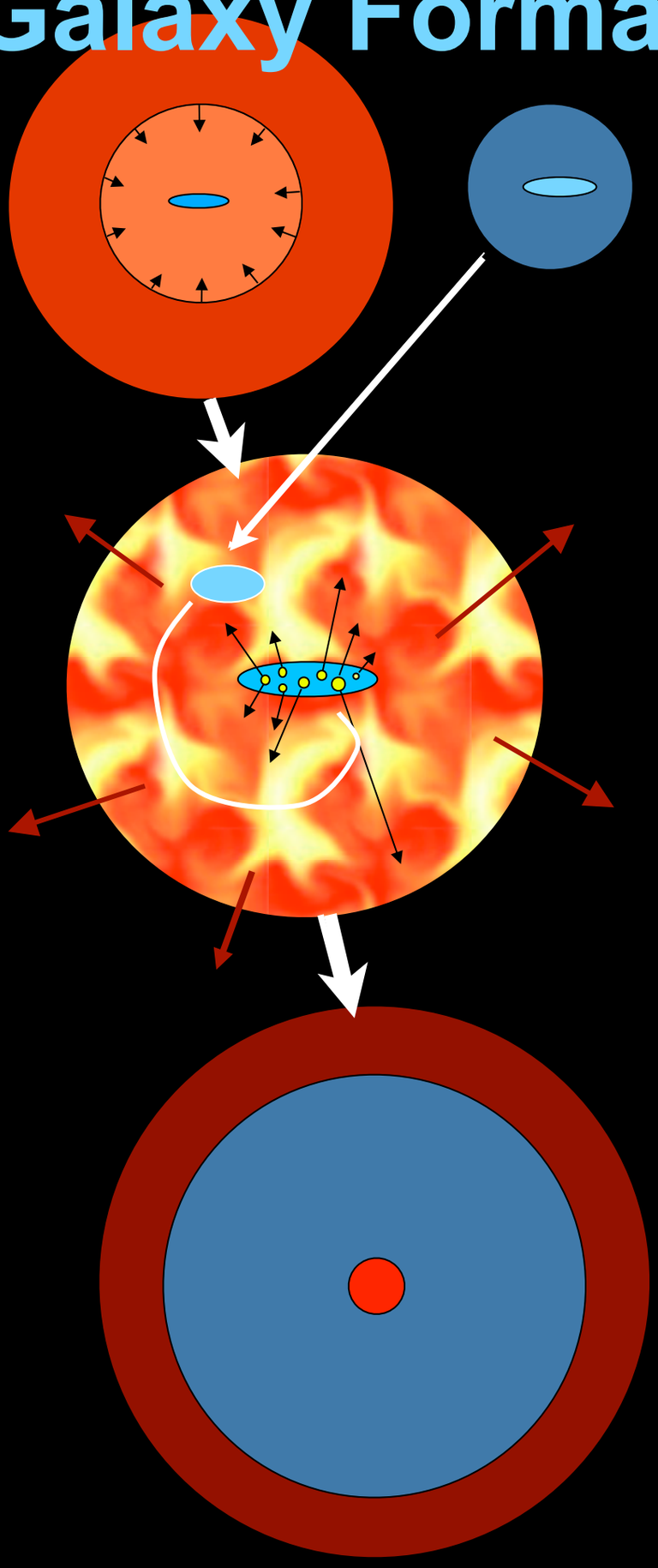

- gas is collisionally heated when perturbations ‘turn around’ and collapse to form gravitationally bound structures
- gas in halos cools via atomic line transitions (depends on density, temperature, and metallicity)
- cooled gas collapses to form a rotationally supported disk
- cold gas forms stars, with efficiency a function of gas density (e.g. Schmidt-Kennicutt Law, metallicity effects?)
- massive stars and SNe reheat (and in small halos expel) cold gas and some metals
- galaxy mergers trigger bursts of star formation; ‘major’ mergers transform disks into spheroids and fuel AGN
- AGN feedback cuts off star formation
- **including effects of dissipation in gas-rich galaxy mergers leads to observed elliptical size-mass relation**
- **including spheroid formation by disk instability is essential to reproduce the observed elliptical luminosity function**

White & Frenk 91; Kauffmann+93; Cole+94; Somerville & Primack 99; Cole+00; Somerville, Primack, & Faber 01; Croton et al. 2006; Somerville +08; Fanidakis+09; Covington et al. 10, 11; Somerville, Gilmore, Primack, & Dominguez 11; Porter et al.

Semi-Analytic Models Based on the Bolshoi Simulation

- Elliptical galaxies follow a size-mass relation. Our semi-analytic model correctly predicts this and the other scaling relations of elliptical galaxies.

- Disk galaxies follow a relation between their rotation velocity and their luminosity. The model also correctly predicts this.

- Our semi-analytic model also correctly predicts the numbers of Disk galaxies and Elliptical galaxies of all masses.

Semi-Analytic Models Based on the Bolshoi Simulation

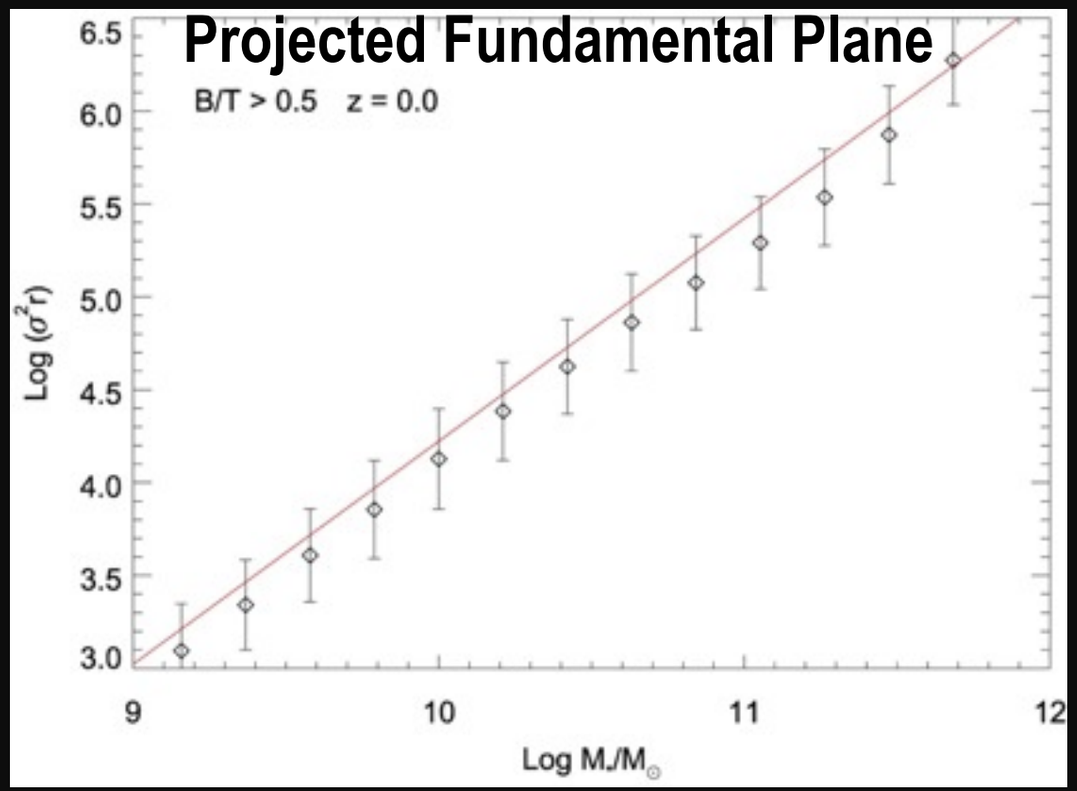

- Elliptical galaxies follow a size-mass relation. The theory correctly predict this and the other observed relations of elliptical galaxies

- With disk instabiliies, the theory correctly predicts the numbers of Disk Galaxies and Elliptical Galaxies of all masses

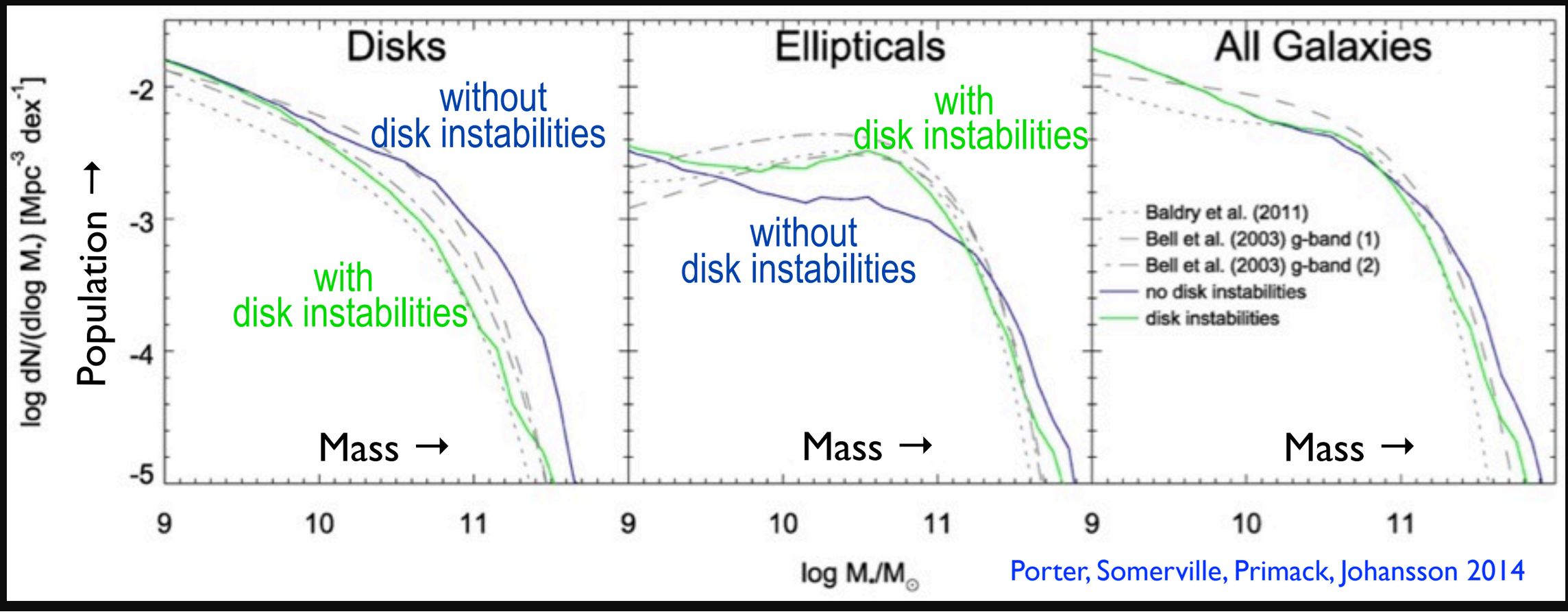

Porter, Somerville, Primack, Johansson 2014

Semi-Analytic Models Based on the Bolshoi Simulation

Porter, Somerville, Primack, Johansson, MNRAS submitted
Porter, Somerville, Croton, Covington, Graves, Faber, Primack, MNRAS submitted (March 2014)

Early-Type Galaxy Fraction

Disk Instability Predictions Agree Better with Data

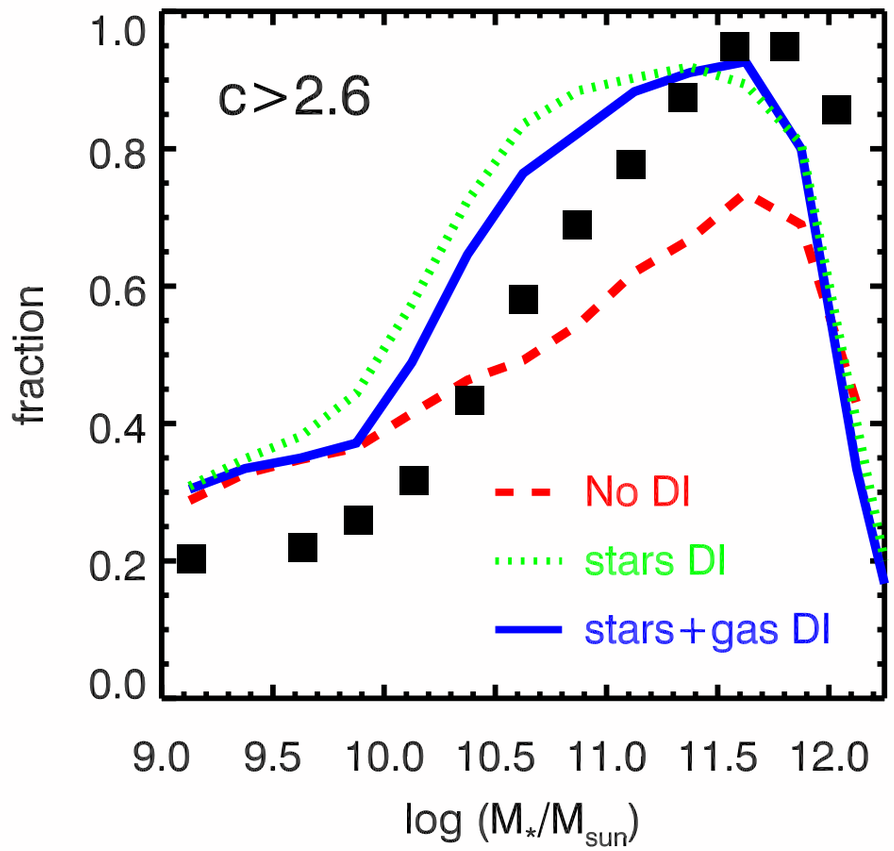

M_{BH} - M_* Relation

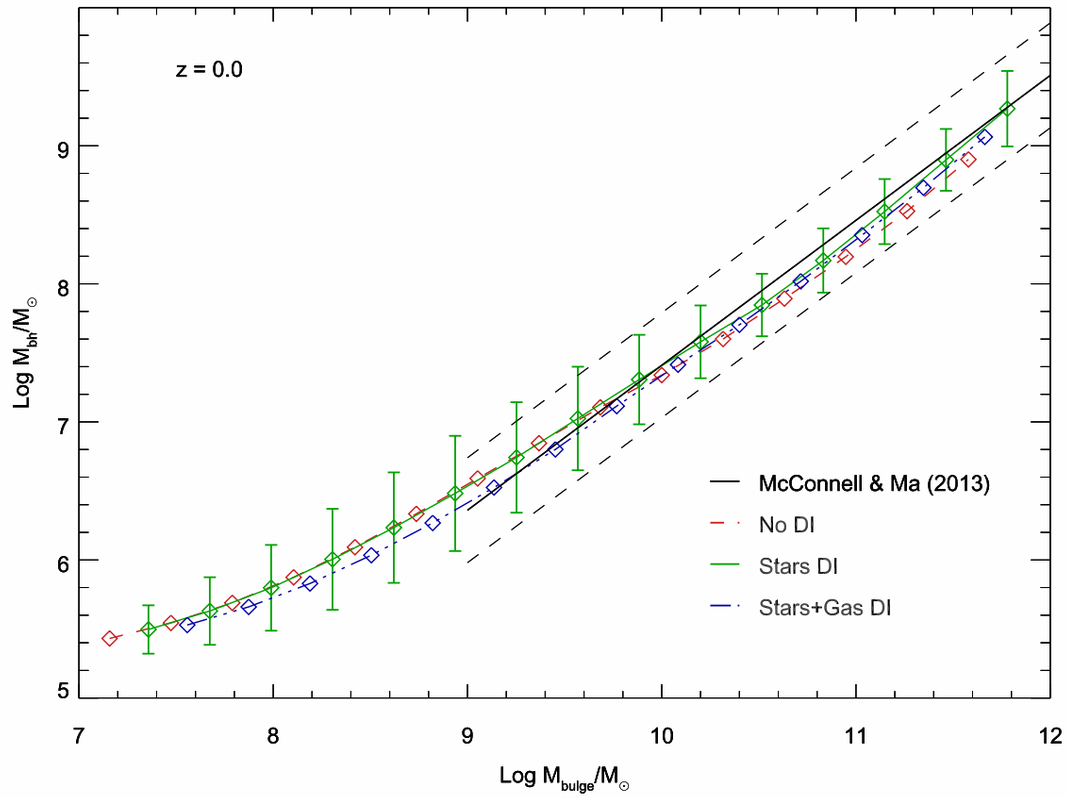

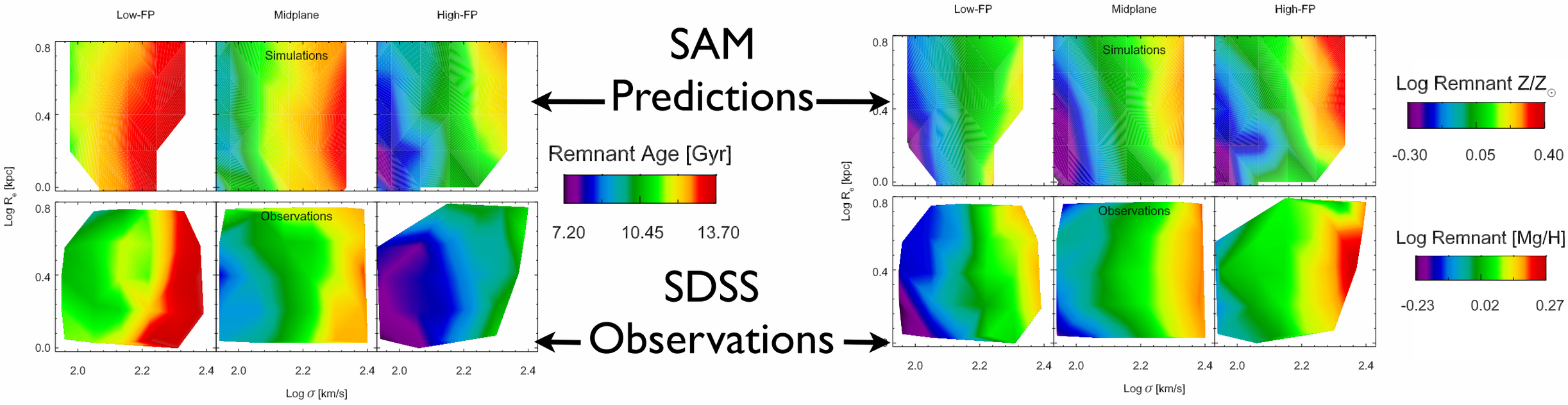

How Galaxies Form Stars and Elements

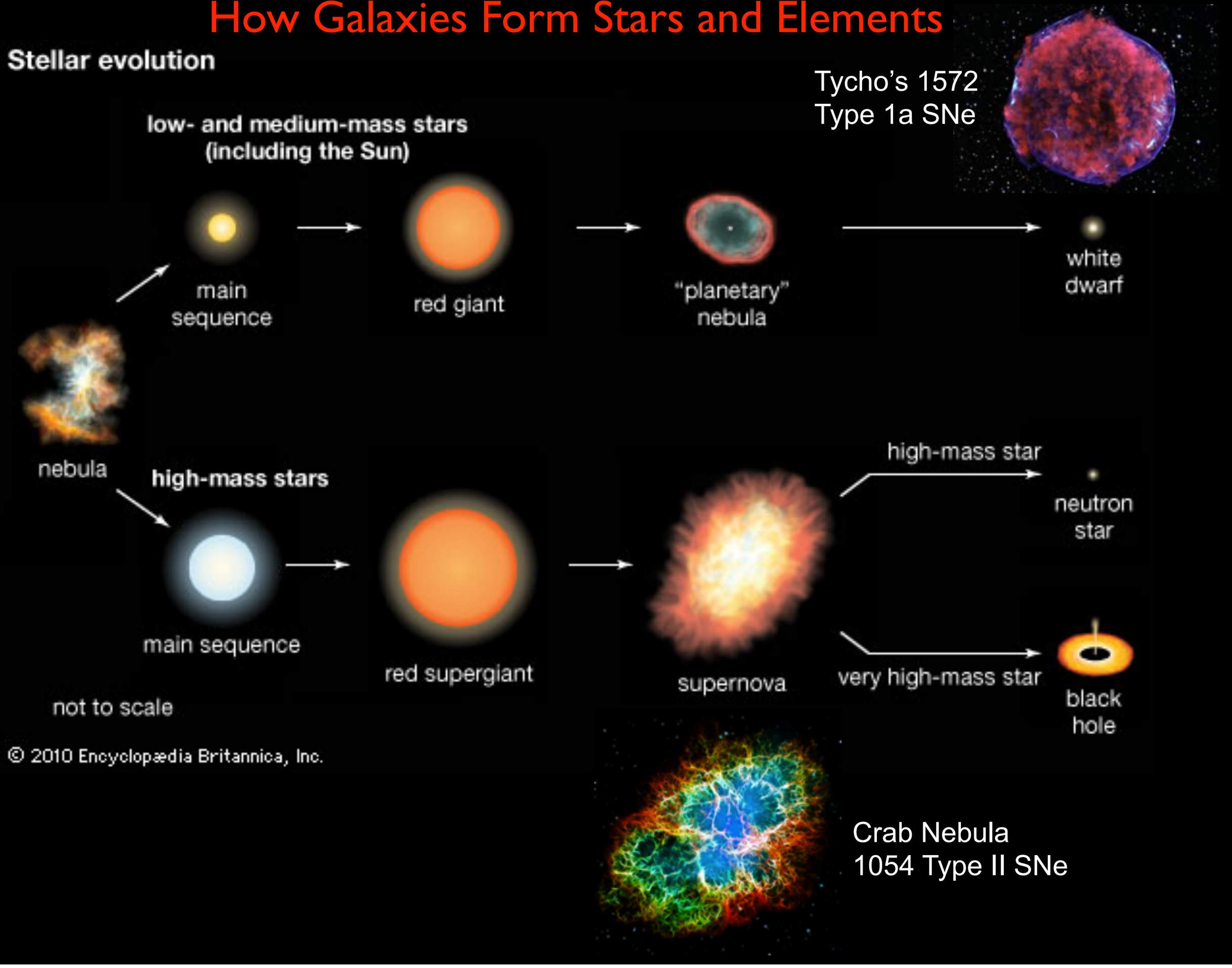

Tycho's 1572
Type 1a SNe

Crab Nebula
1054 Type II SNe

How Galaxies Form Stars and Elements

The sun's energy mainly comes from the *p*–*p* fusion cycle $4p \rightarrow {}^4\mathrm{He} + 2e^+ + 2\nu_e + 26.73$ MeV. This is supressed because of quantum mechanical barrier penetration -- which keeps the sun fusing steadily, rather than exploding like a hydrogen bomb. The fusion rate is proportional to the product of the Maxwell velocity and barrier penetration distributions, and is shown by the solid curve. In addition to the *p*–*p* cycle, another cycle involving the elements C, N, and O accounts for about 1.6% of helium production in the Sun. Since the nuclear charges are larger, this cycle is more important for more massive hydrogen burning stars with higher core temperatures, such as Sirius A.

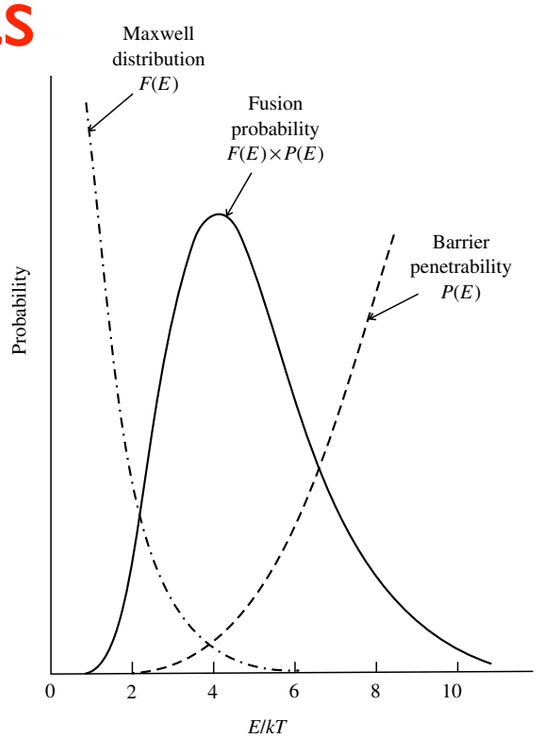

After most of the hydrogen in the stellar core is fused, a massive star's central temperature must grow higher to fuse ^{4}He to ^{12}C, ^{16}O, etc., the α-elements. Other elements are also produced by fusion, e.g. $^{12}\mathrm{C} + {}^{12}\mathrm{C} \rightarrow {}^{20}\mathrm{Ne} + {}^4\mathrm{He}$. Eventually, the core becomes iron, with the highest binding energy per nucleon. Fusion can extract no further energy, so the core collapses. About 99% of the gravitational energy released in such core-collapse supernovas escapes in a burst of neutrinos. Detection the expected numbers and energies of neutrinos from the supernova 1987A in the Large Magellanic Cloud confirmed this basic theory -- see Perkins section 10.9. Stars that star mofe massive than about $8M_\odot$ end their lives as core-collapse supernovae, which result in neutron stars or (for the most massive ones) black holes.

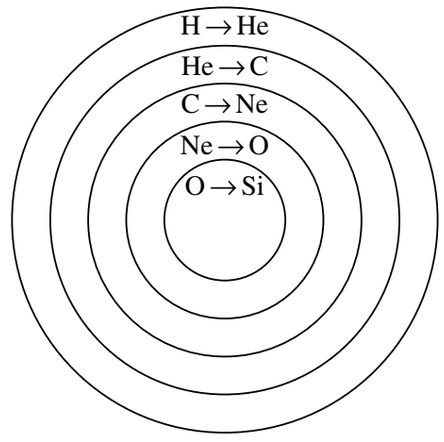

Elements more massive than iron are formed mainly by the r-process, in which neutrons rapidly join outgoing nuclei, which are simultaneously beta-decaying. The abundance of the heavy nuclei is thus determined by competition between neutron accretion and beta-decay. The r-process also occurs in merging neutron stars.

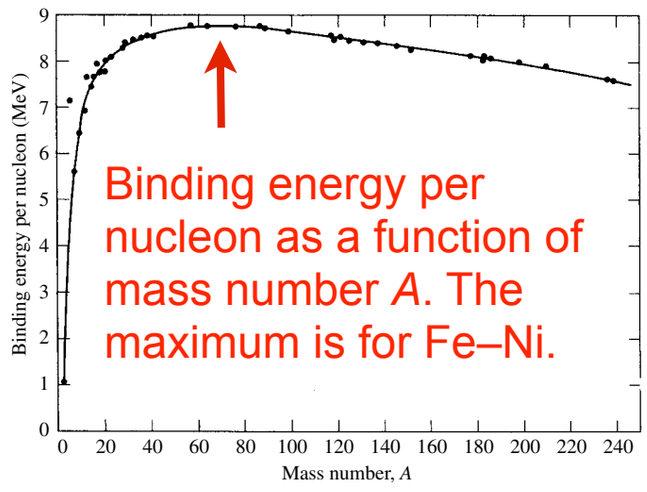

Binding energy per nucleon as a function of mass number *A*. The maximum is for Fe–Ni.

nucleosynthesis of the heavy elements

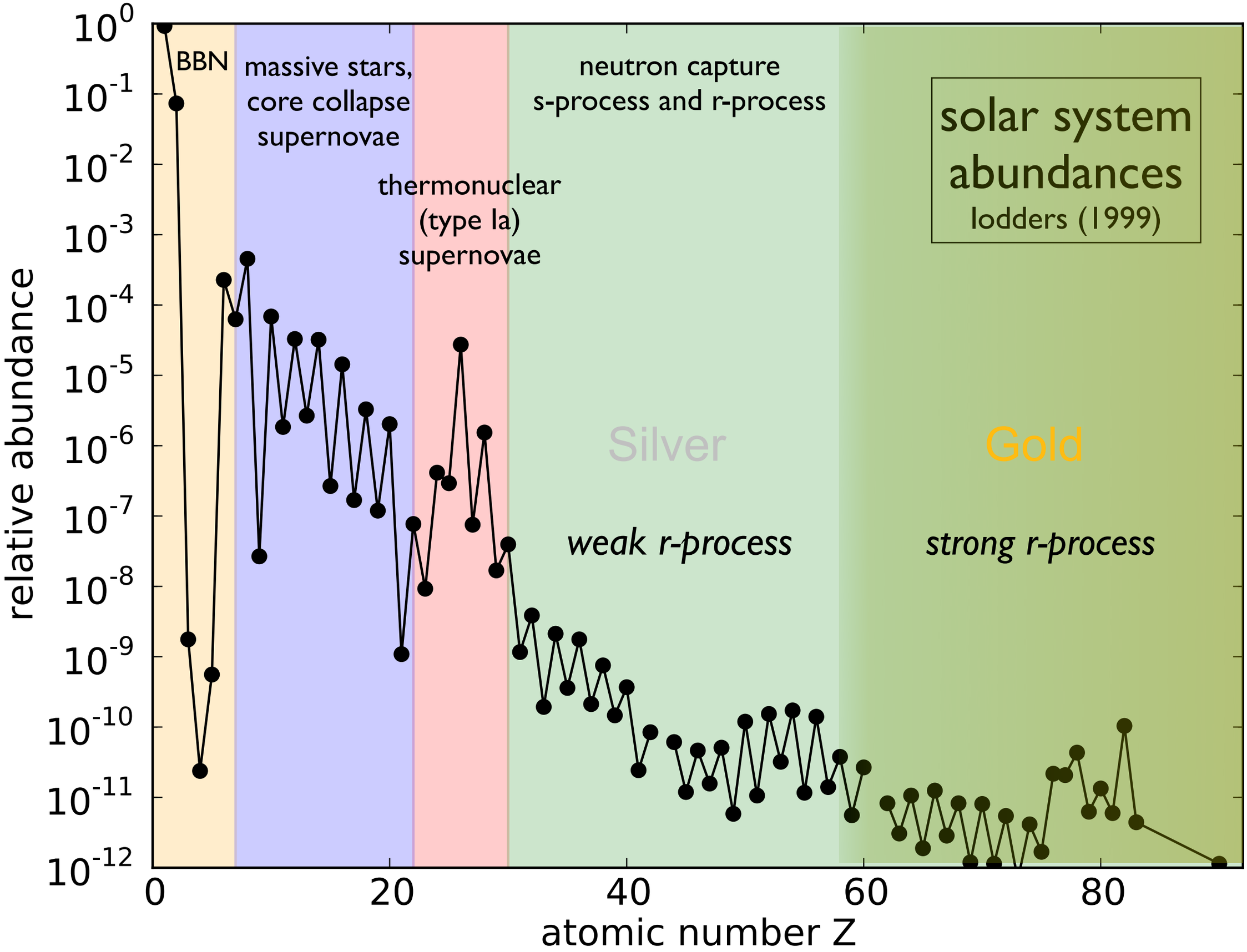

possible r-process sites

need neutron rich ejecta: $Y_e = n_p/(n_n + n_p) < 0.5$

core-collapse supernovae

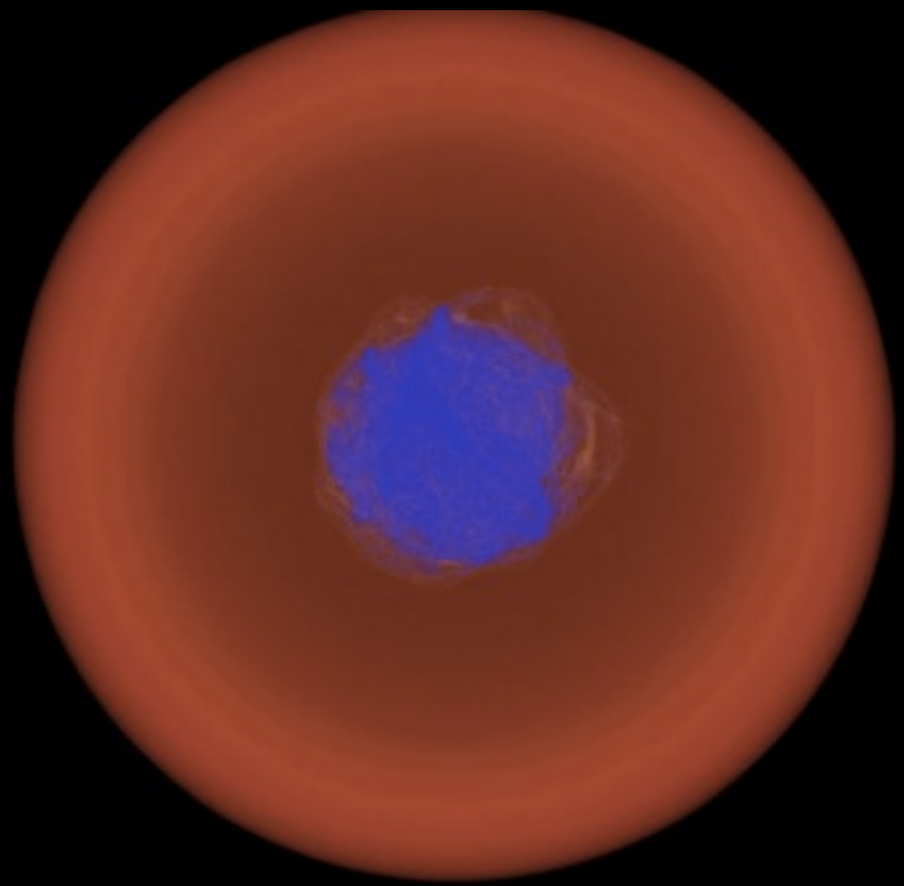

neutrino driven wind from
a proto-neutron star

small ejected mass (~10^{-6} -10^{-5} M_{sun}?)
but high rate

neutron star merger

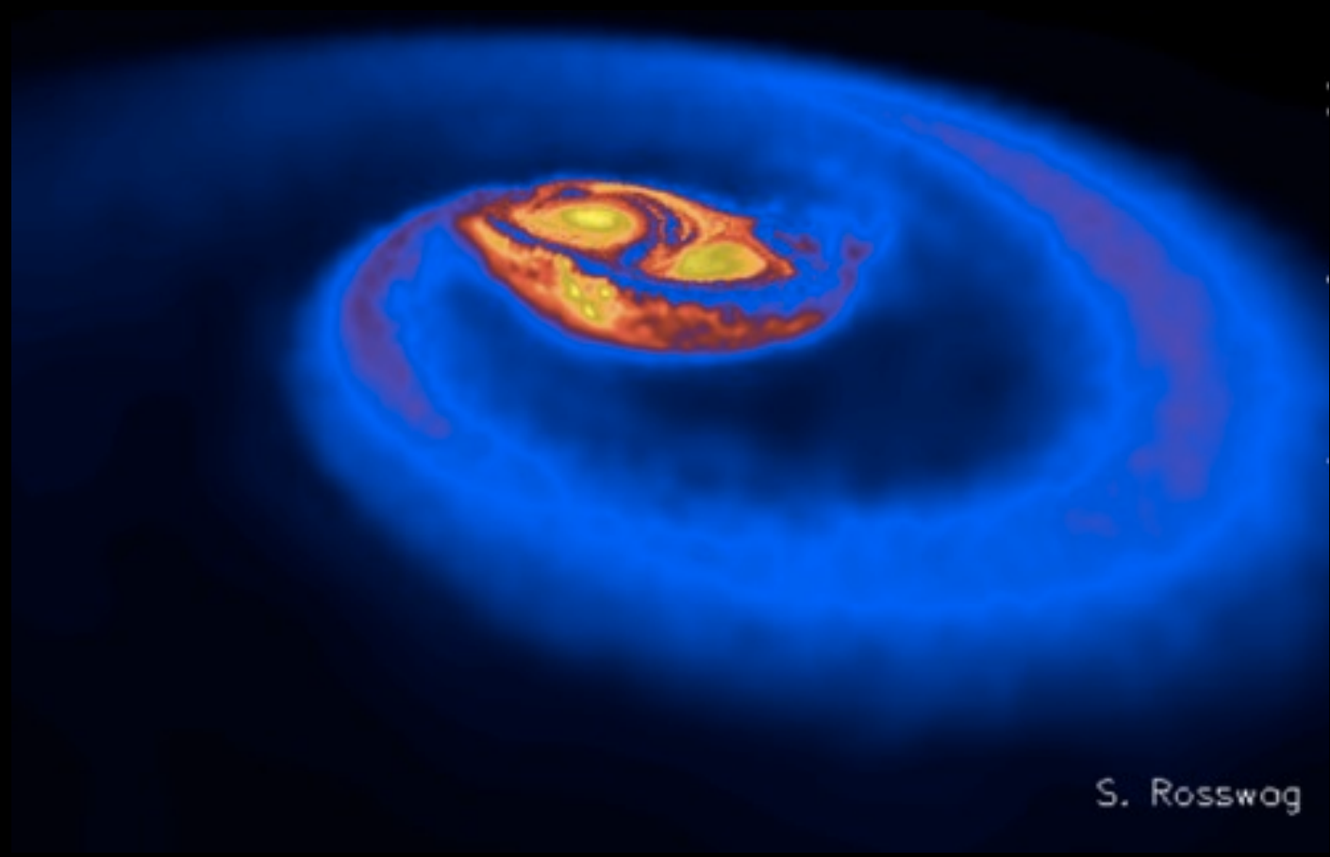

dynamical ejecta
or disk winds

larger ejected mass (~10^{-4} -10^{-2} M_{sun}?)
but much lower rate

the r-process

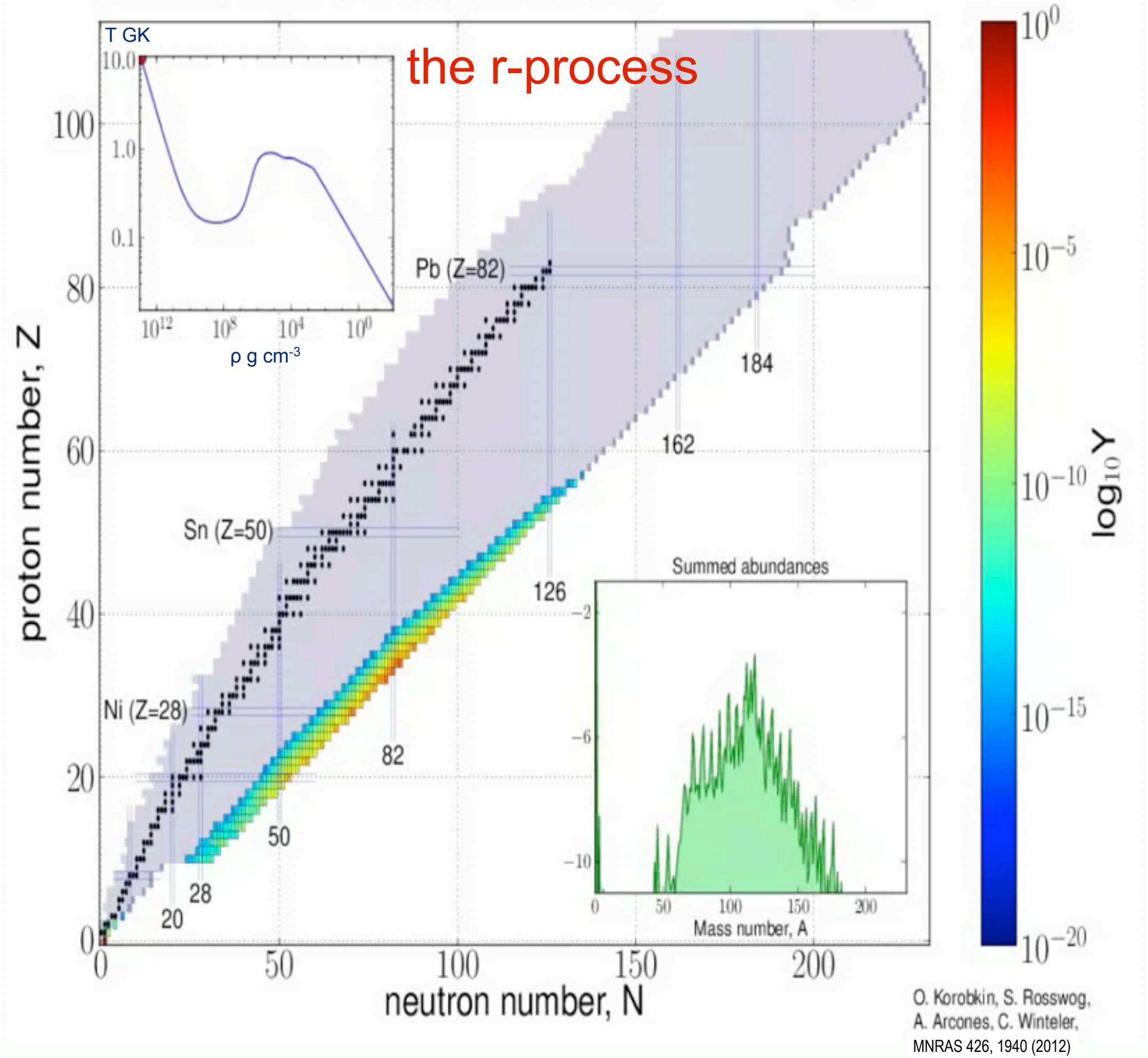

O. Korobkin, S. Rosswog,
A. Arcones, C. Winteler,
MNRAS 426, 1940 (2012)

Type Ia Supernovae - Exploding White Dwarfs

At high densities, such as occur in stellar cores of stars that start with < 8 $M_\odot$ at an advanced stage of evolution, a new form of pressure, in addition to gas pressure and radiation pressure, called *electron degeneracy pressure*, becomes important. To investigate the role of this degeneracy pressure, consider a gas of electrons at absolute zero temperature. The electrons will fall into quantum states of the lowest possible energy, and for this reason the gas is said to be degenerate. The Pauli exclusion principle applies to such identical fermions, so that each quantum state can be occupied by one electron only. At zero temperature, the energy is minimized if all the states are occupied, up to some maximum energy called the Fermi energy εF, and all states of energy ε > εF are unoccupied (see Figure at right). The corresponding momentum is called the Fermi momentum p_F. For values of temperature T above zero, not all these quantum states are filled and the energy spectrum extends above the Fermi energy. Ultimately, when $kT >> \varepsilon F$, the energy distribution reverts to the Fermi–Dirac distribution. When the electrons are non-relativistic, their pressure can support the collapsed star -- a white dwarf. But the electrons become relativistic if the white dwarf mass exceeds $M_{Chandra} \approx 1.4\ M_\odot$, known as the Chandrasekhar mass, and the white dwarf explodes as a Type Ia SNe, producing ~ 0.5 $M_\odot$ of cobalt, nickel, and iron. Most of the iron-group elements are produced by Type Ia SNe.

Type Ia SNe can result from accretion of gas by a white dwarf (called a “single-degenerate” process) or merger to two white dwarfs (“double-degenerate” process). Several double-degenerate Type Ia SNe have been observed, and may even represent a majority of Type Ia SNe. Type Ia SNe can be normalized and used as distance indicators, since there is an empirical relation between the length of time to brighten and dim and the absolute peak luminosity.

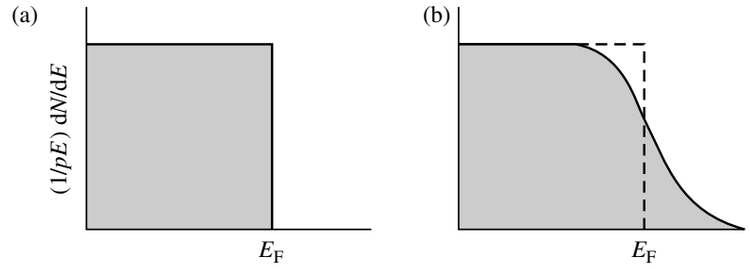

Distribution of electron energies (a) for an electron gas at absolute zero temperature, with all levels filled up to the Fermi energy; and (b) for an electron gas at finite, low temperature, where electrons begin to spill over into states above the Fermi energy.

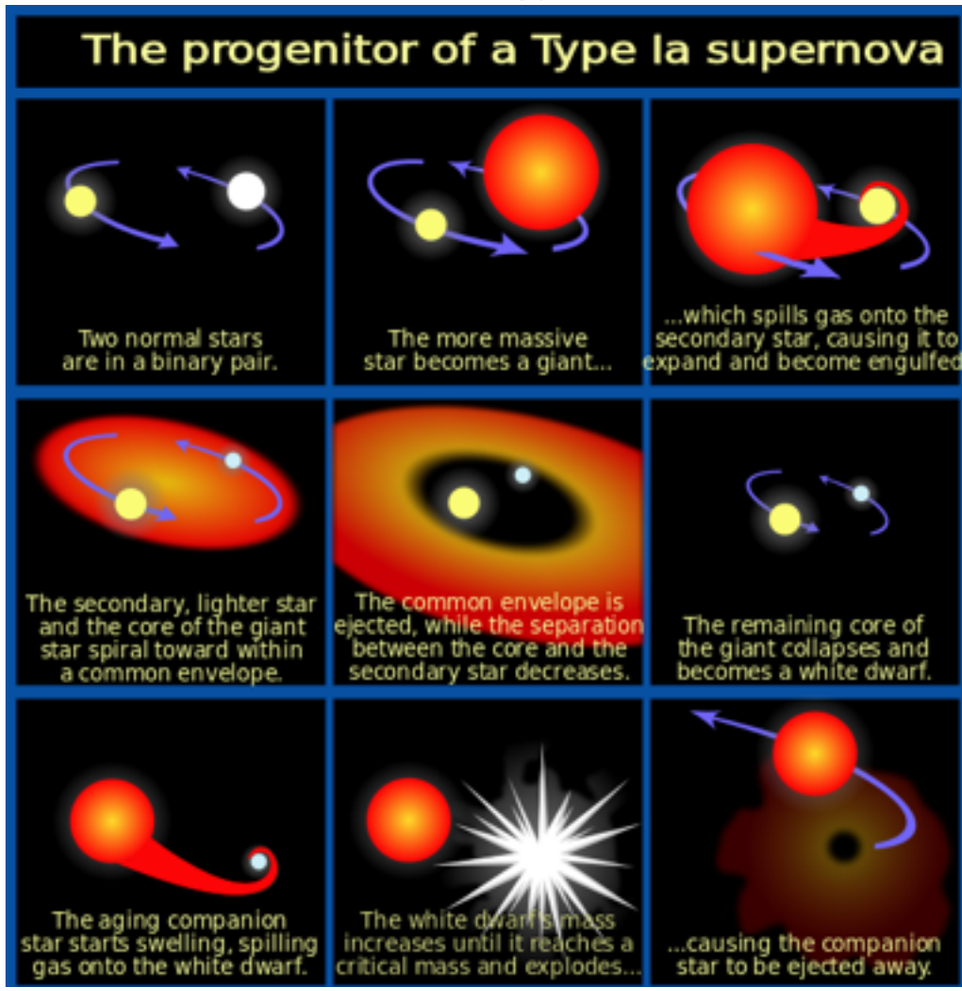

Frank Summers, STScI: “Cosmic Collisions Galore”

http://hubblesite.org/newscenter/archive/releases/2008/16/video/d/

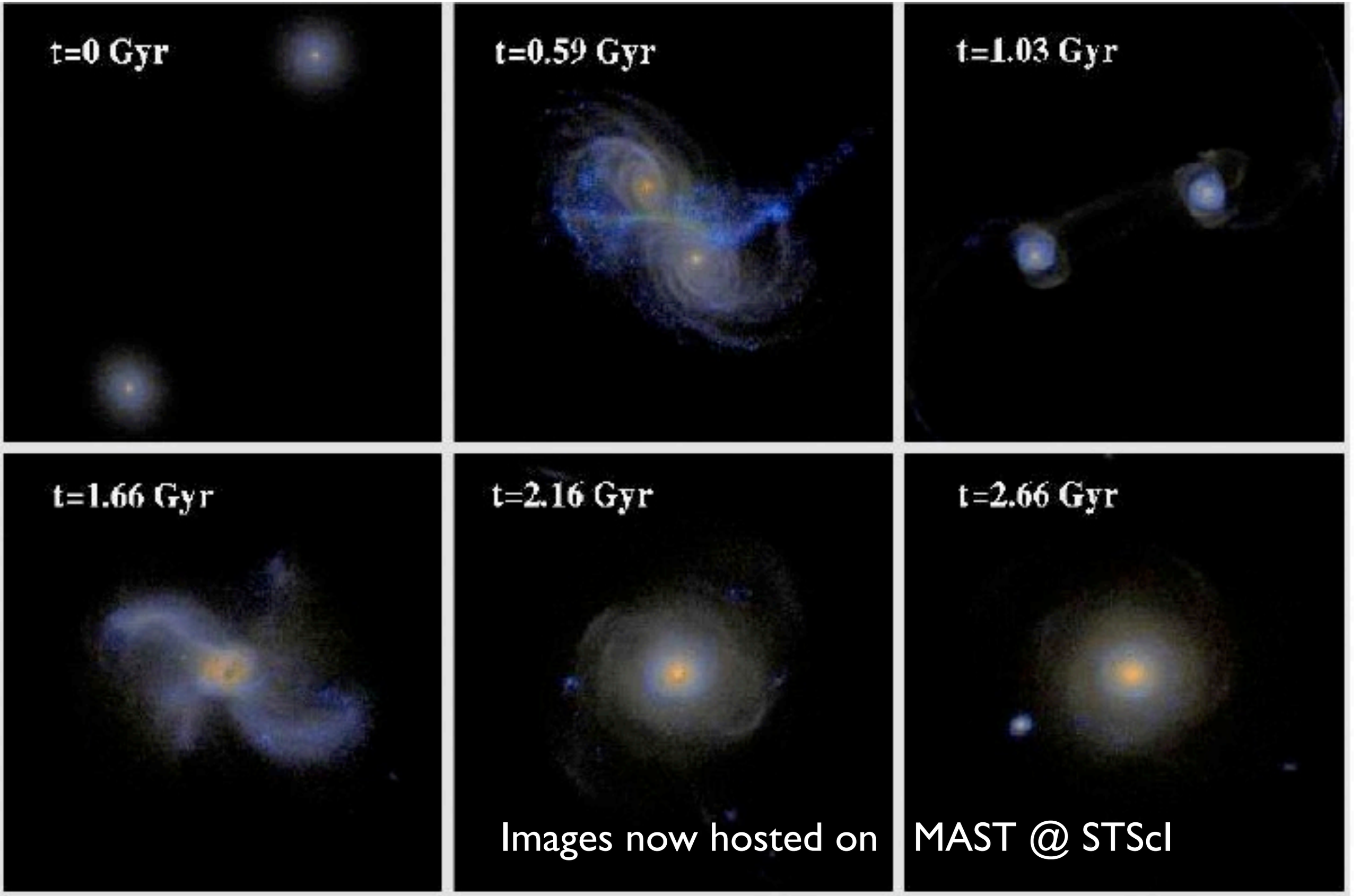

Lotz, Jonsson, Cox, Primack 2008 Galaxy Merger Morphologies and Time-Scales from Simulations analyzed to determine observability timescales using CAS, G-M_{20}, pairs ➙ merger rates

The Astrophysical Journal, 742:103 (22pp), 2011 December 1

THE MAJOR AND MINOR GALAXY MERGER RATES AT $z < 1.5$

Jennifer M. Lotz[1,2,9], Patrik Jonsson[3], T. J. Cox[4,10], Darren Croton[5], Joel R. Primack[6], Rachel S. Somerville[2,7], and Kyle Stewart[8,11]

ABSTRACT

Calculating the galaxy merger rate requires both a census of galaxies identified as merger candidates and a cosmologically averaged "observability" timescale $\langle T_{\rm obs}(z)\rangle$ for identifying galaxy mergers. While many have counted galaxy mergers using a variety of techniques, $\langle T_{\rm obs}(z)\rangle$ for these techniques have been poorly constrained. We address this problem by calibrating three merger rate estimators with a suite of hydrodynamic merger simulations and three galaxy formation models. We estimate $\langle T_{\rm obs}(z)\rangle$ for (1) close galaxy pairs with a range of projected separations, (2) the morphology indicator $G - M_{20}$, and (3) the morphology indicator asymmetry A. Then, we apply these timescales to the observed merger fractions at $z < 1.5$ from the recent literature. When our physically motivated timescales are adopted, the observed galaxy merger rates become largely consistent. The remaining differences between the galaxy merger rates are explained by the differences in the ranges of the mass ratio measured by different techniques and differing parent galaxy selection. The major merger rate per unit comoving volume for samples selected with constant number density evolves much more strongly with redshift ($\propto (1+z)^{+3.0\pm1.1}$) than samples selected with constant stellar mass or passively evolving luminosity ($\propto (1+z)^{+0.1\pm0.4}$). We calculate the minor merger rate ($1{:}4 < M_{\rm sat}/M_{\rm primary} \lesssim 1{:}10$) by subtracting the major merger rate from close pairs from the "total" merger rate determined by $G - M_{20}$. The implied minor merger rate is $\sim$3 times the major merger rate at $z \sim 0.7$ and shows little evolution with redshift.

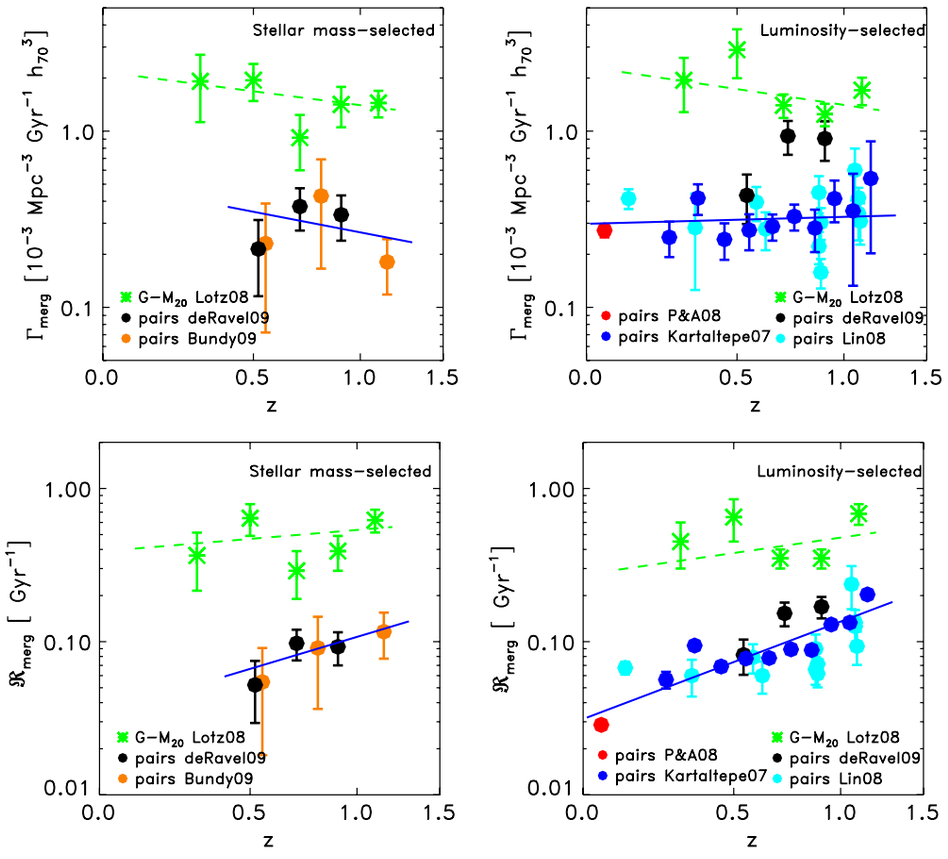

Figure 10. Top: $\Gamma_{\rm merg}$, the merger rate per comoving unit volume, for close pairs (circles) and G – M20 (asterisks), for stellar-mass-selected (left) and rest-frame luminosity-selected samples. Bottom: $R_{\rm merg}$, the fractional merger rate, for close pairs (circles) and G – M20 (asterisks), for the same samples. The error bars are computed using the observational uncertainties on $f_{\rm merg}$, $f_{\rm pair}$, and $n_{\rm gal}$ and do not include uncertainties in $\langle T_{\rm obs}\rangle$. G – M20 probes both major and minor mergers, and therefore captures a "total" merger rate, which is several times higher than the major merger rate probed by these close pair studies. The evolution in $\Gamma_{\rm pairs}(z)$ is weaker than in $R_{\rm pairs}(z)$ because $f_{\rm pairs}$ increases with redshift (Figure 1) while the corresponding $n_{\rm gal}$ decreases with redshift for fixed stellar mass and PLE galaxy selections (Figure 2). The best-fit slopes for the close pair (major) merger rates (blue solid lines) are given in Section 5.1 and the best slopes for the G – M20 (total) merger rates (green dashed lines) are given in Section 5.2.

Baryons in Dark Matter Halos

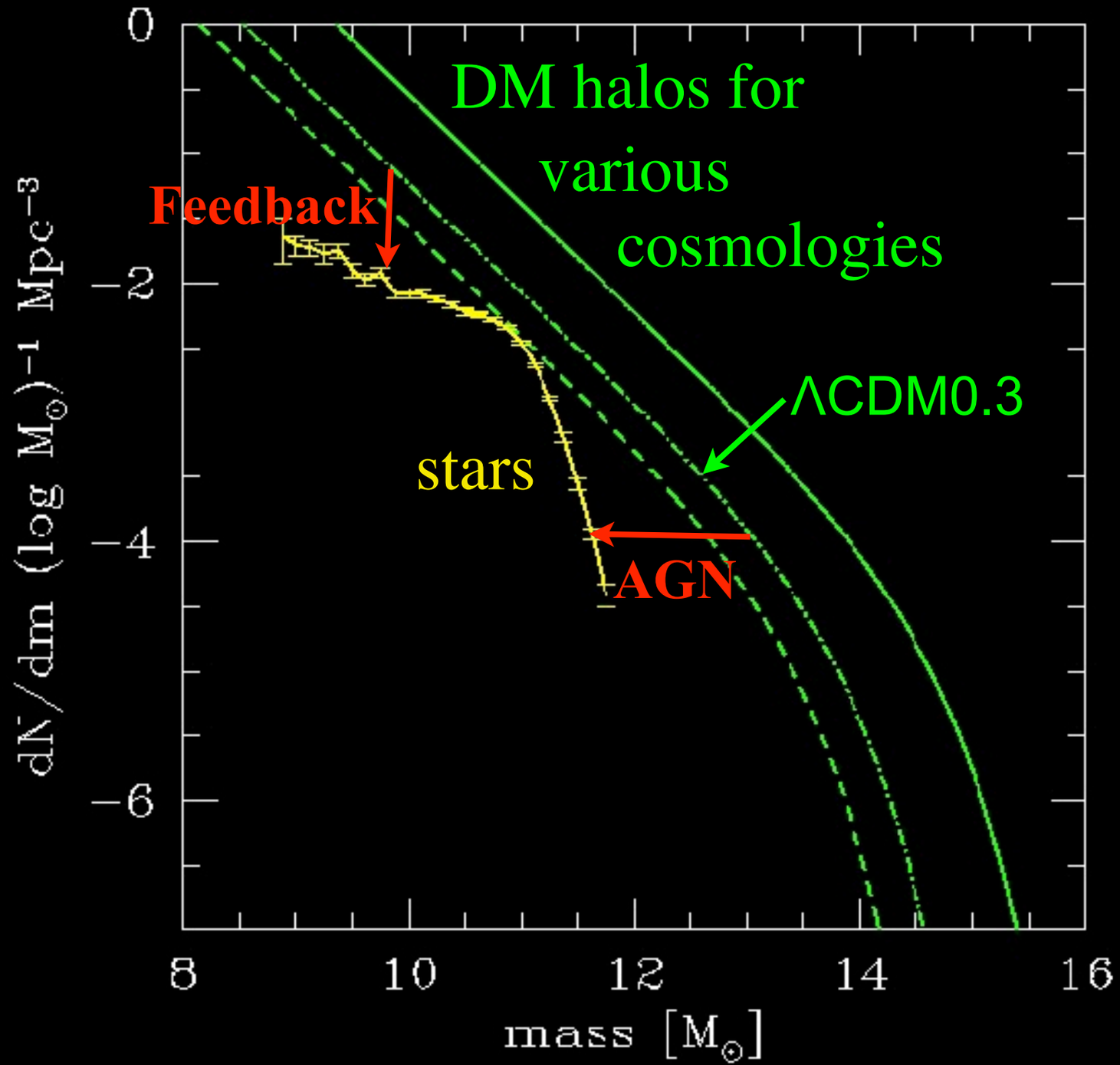

- in order to reconcile CDM (sub)halo mass function with galaxy LF or stellar MF, cooling/star formation must be inefficient overall, most efficient at $M_{halo} \sim 10^{11}\ M_{sun}$
- baryon/DM ratio must be a strongly non-linear (& non-monotonic) function of halo mass

Somerville & Primack 1999; cf. Benson et al. 2003

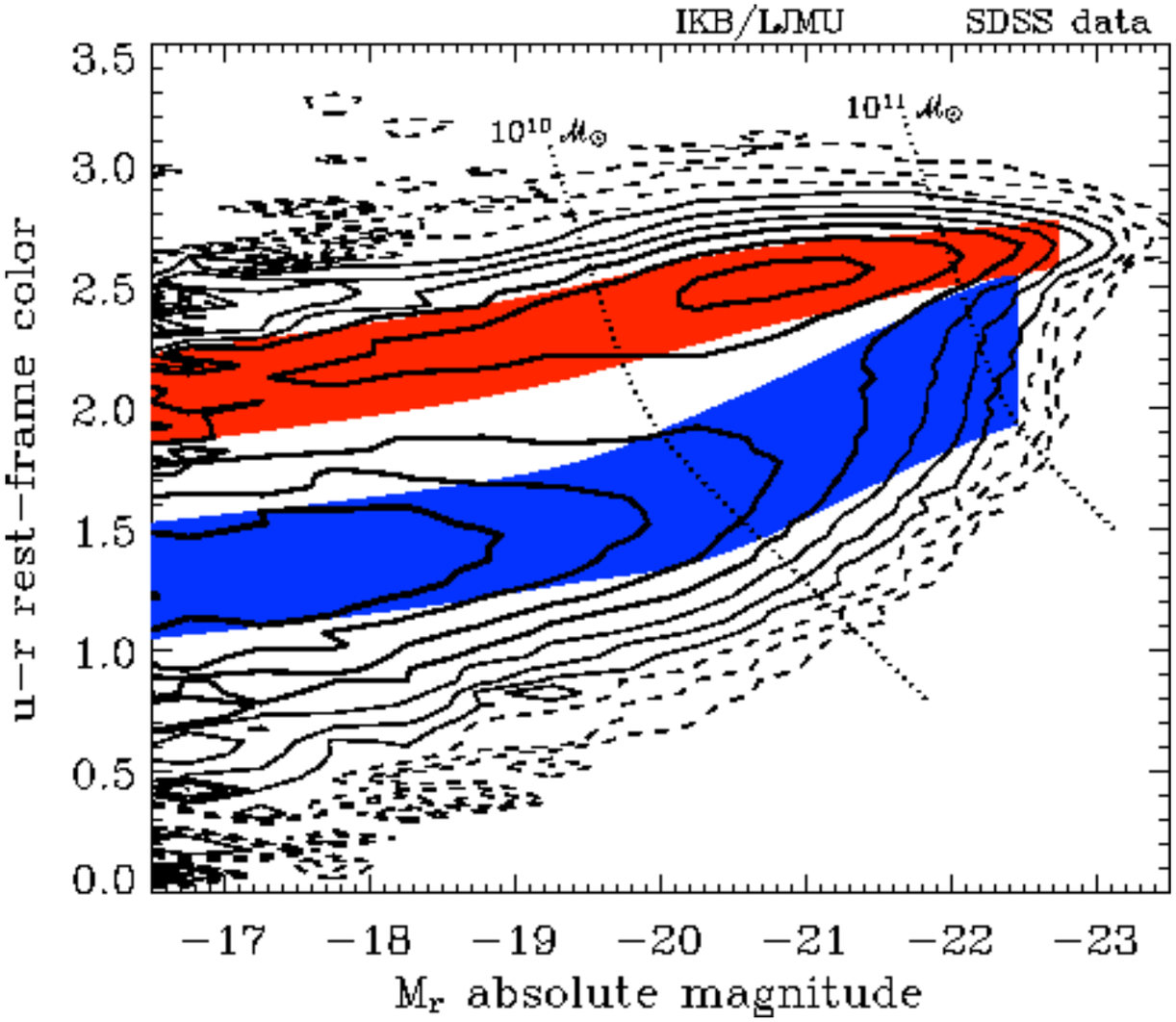

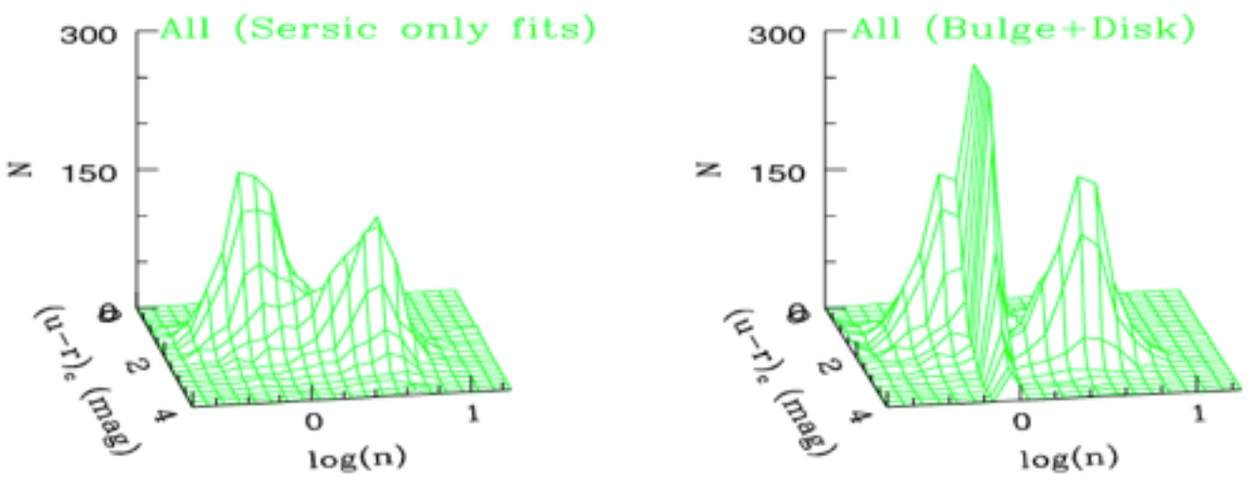

Galaxy bimodality in the color-structure plane (S. Driver et al. 2006)

Color bimodality of galaxies on color-magnitude plot from Baldry et al. (2004). The black solid and dashed contours represent the number density of galaxies: logarithmically spaced with four contours per factor of ten. The distribution is bimodal: there are two peaks corresponding to a red sequence (generally early types) and a blue sequence (late types).

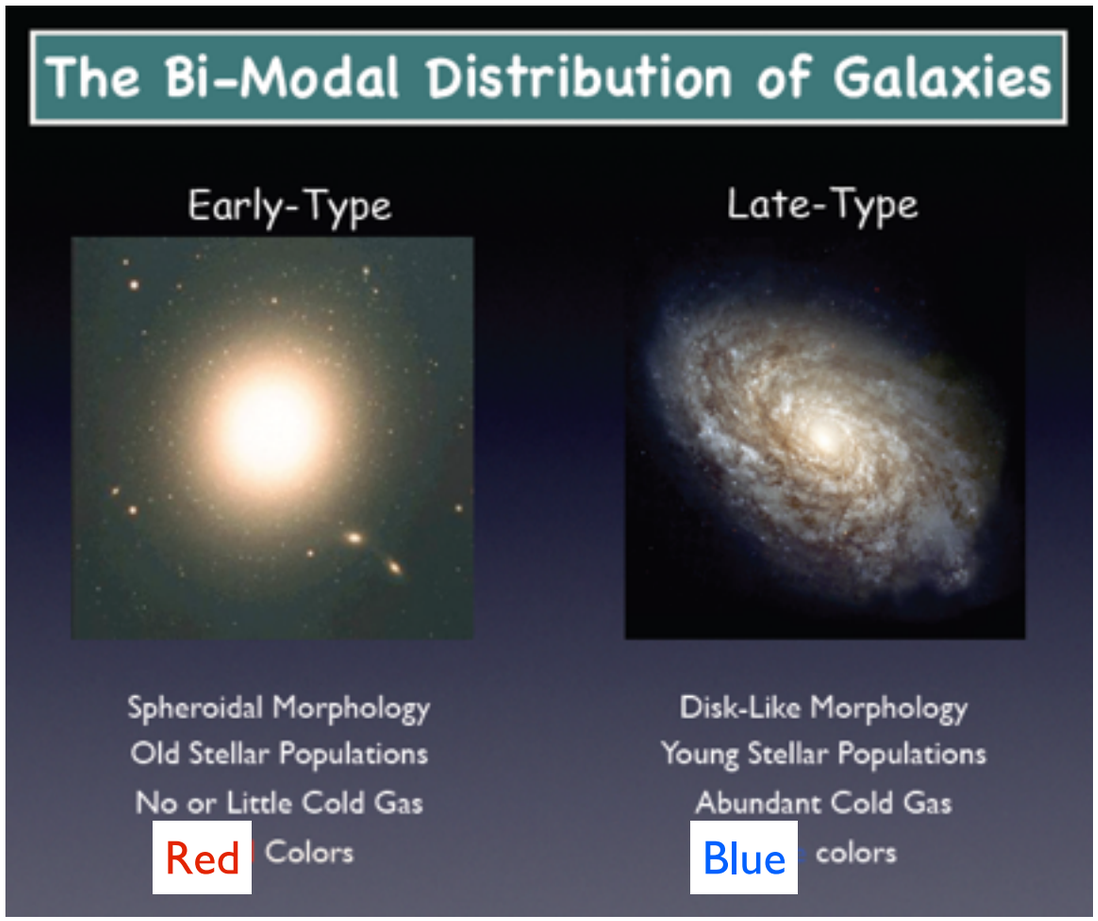

Flow through the color-mass diagram for "central" galaxies

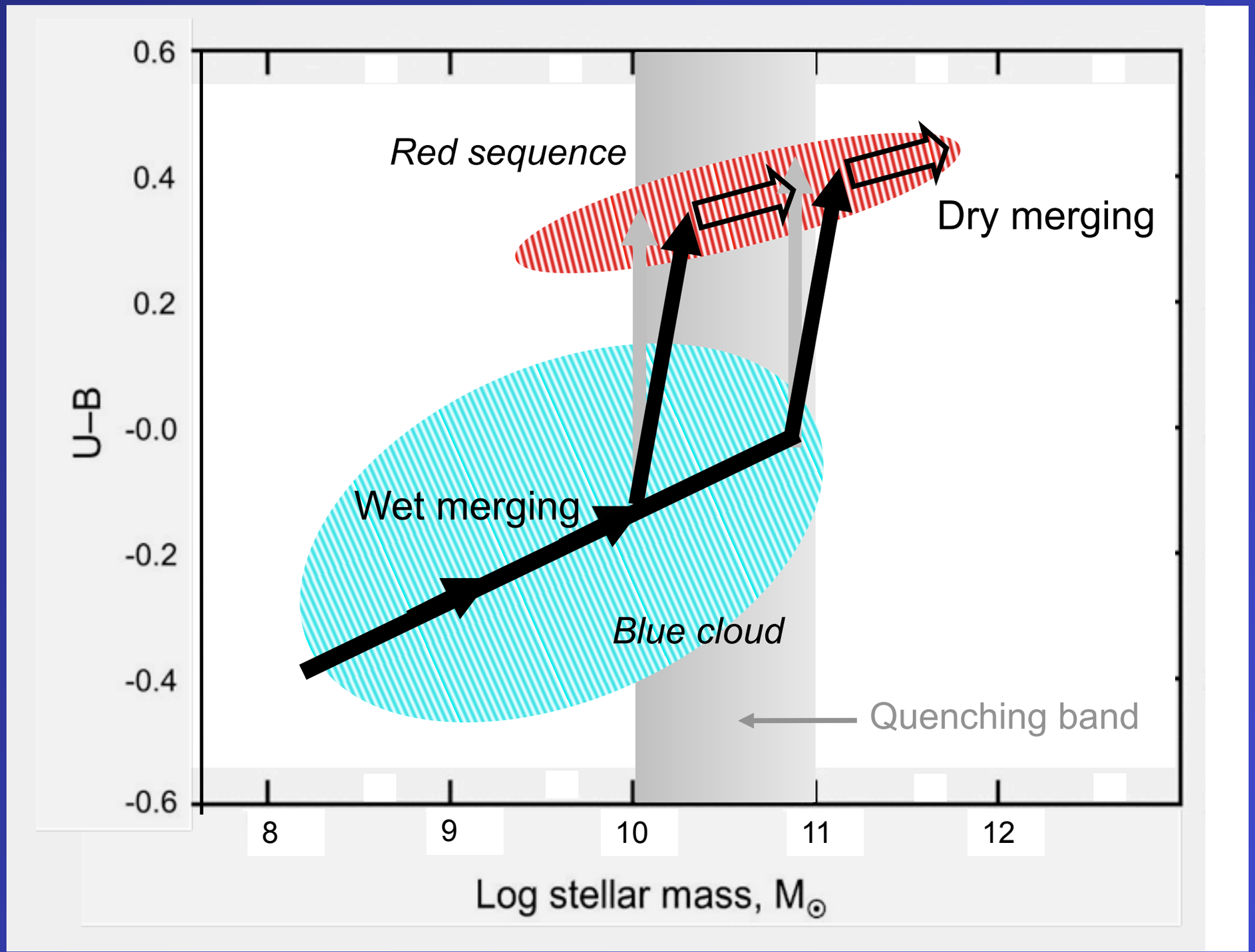

Sandra Faber

Flow through the color-mass diagram for "satellite" galaxies

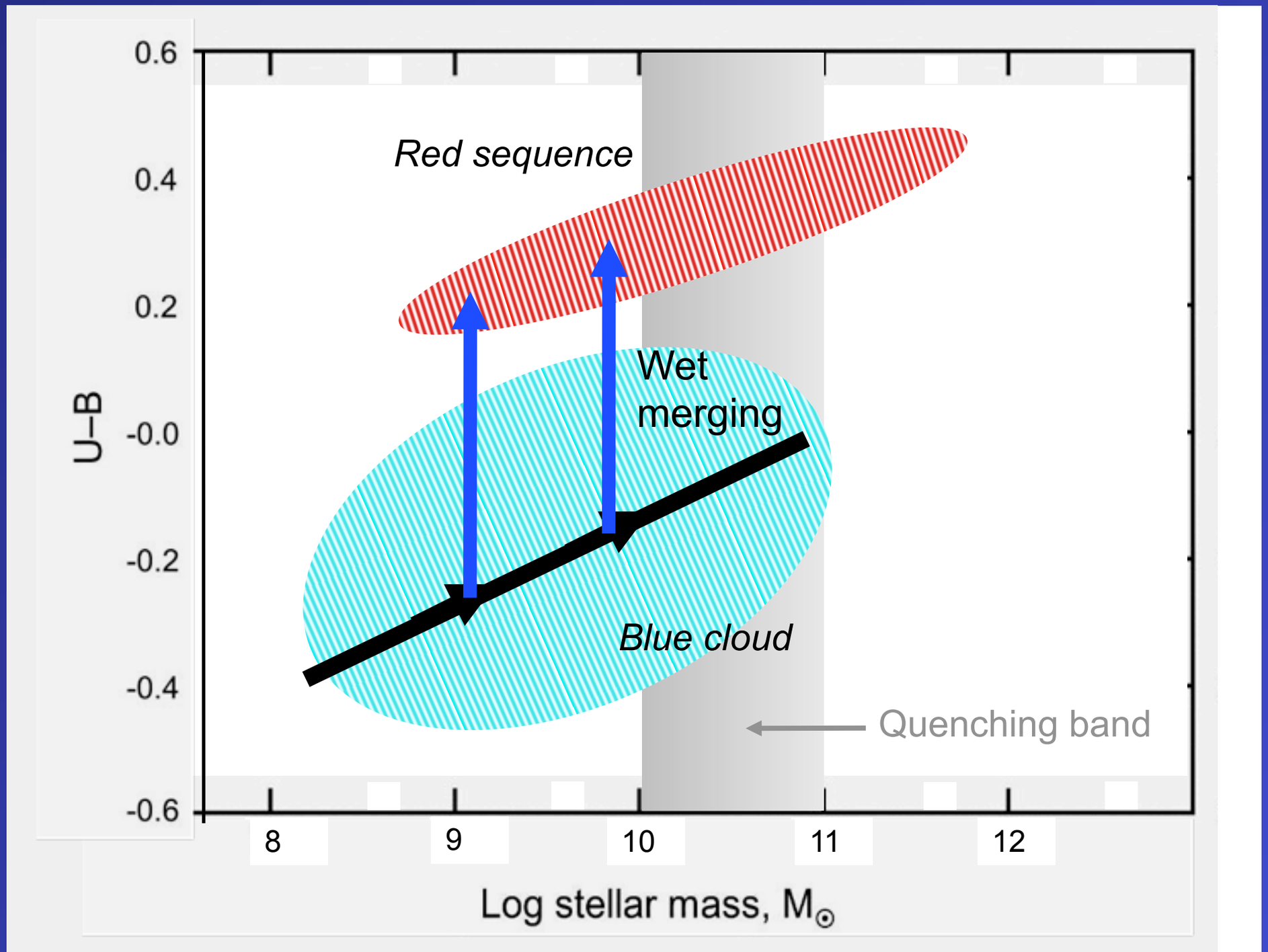

Sandra Faber

Flow through the CM diagram versus environment

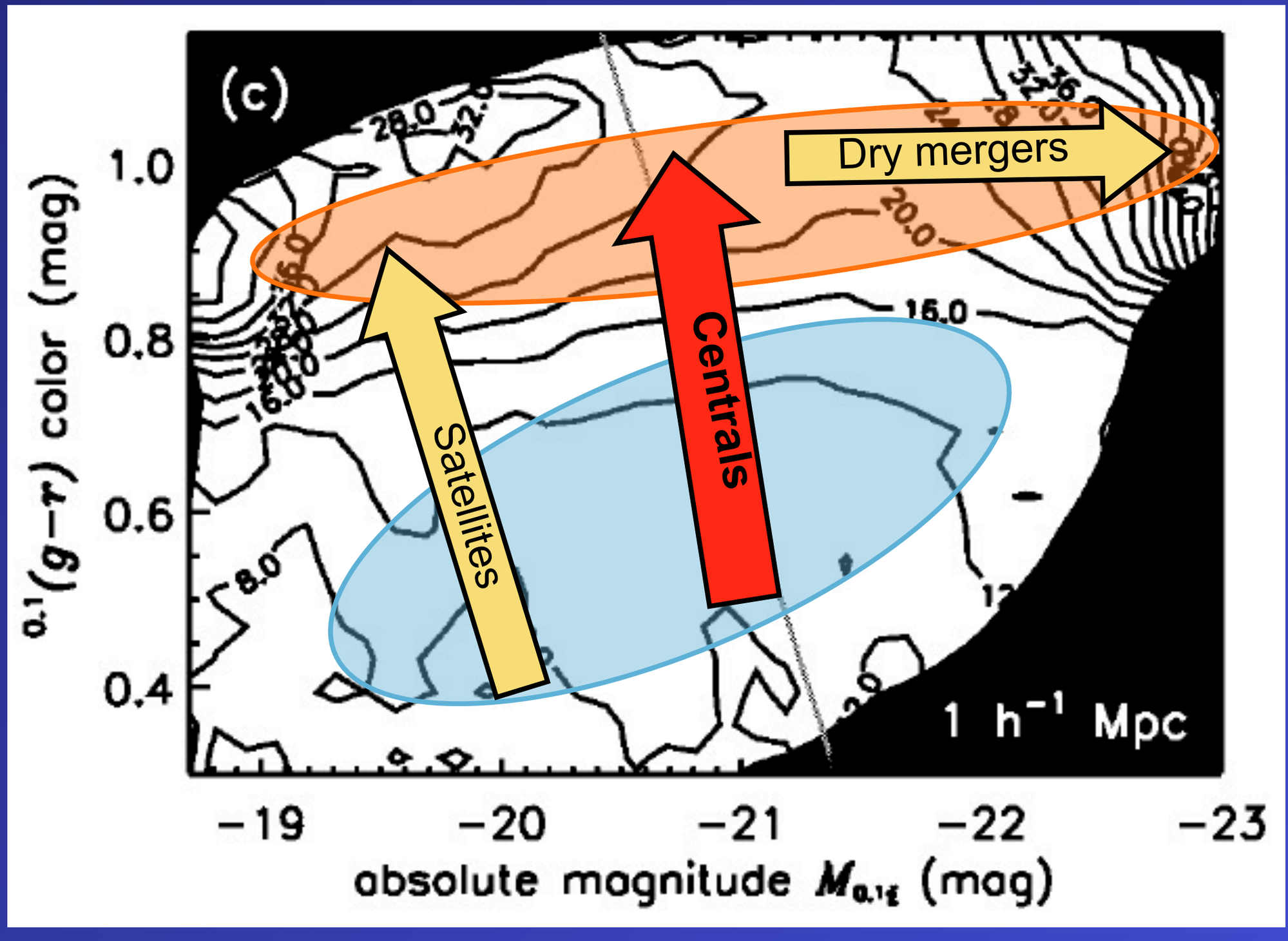

Hogg et al. 2003: Sloan Survey

All formed by environment

no BH

$M_i^{0.1} = -19.3$

Transition mass $3 \times 10^{10}\ M_\odot$

$M_i^{0.1} \sim -21.0$

Satellite/Central wet/dry transition

$M_i^{0.1} > -22.1$

All boxy/dry

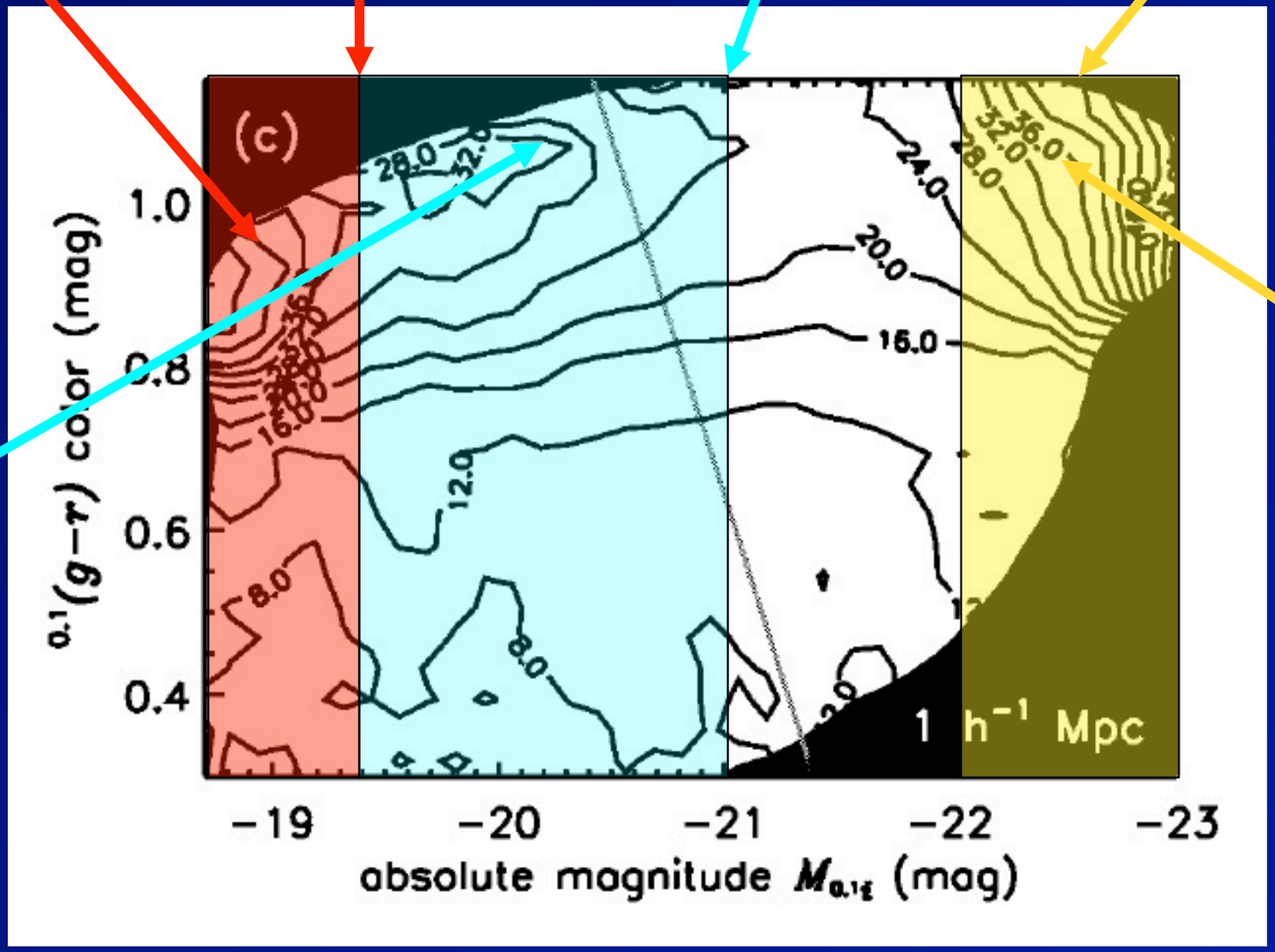

Some by env, some by wet mergers

All by dry mergers

Sandra Faber

Some Results from our Semi-Analytic Models

z=0-2 Luminosity Density

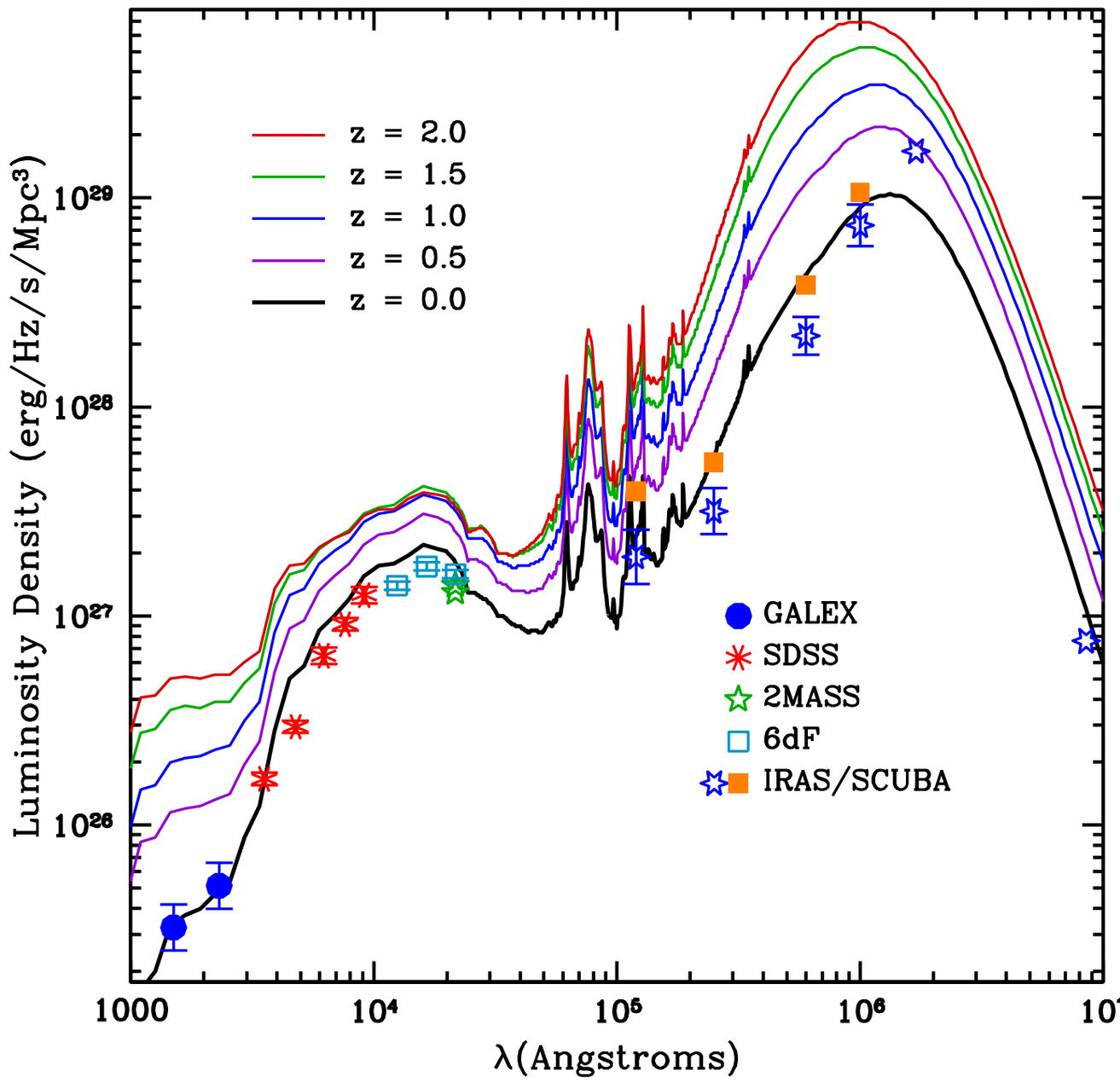

Somerville, Gilmore, Primack, & Dominguez (2012)

z=0-8 Luminosity Density

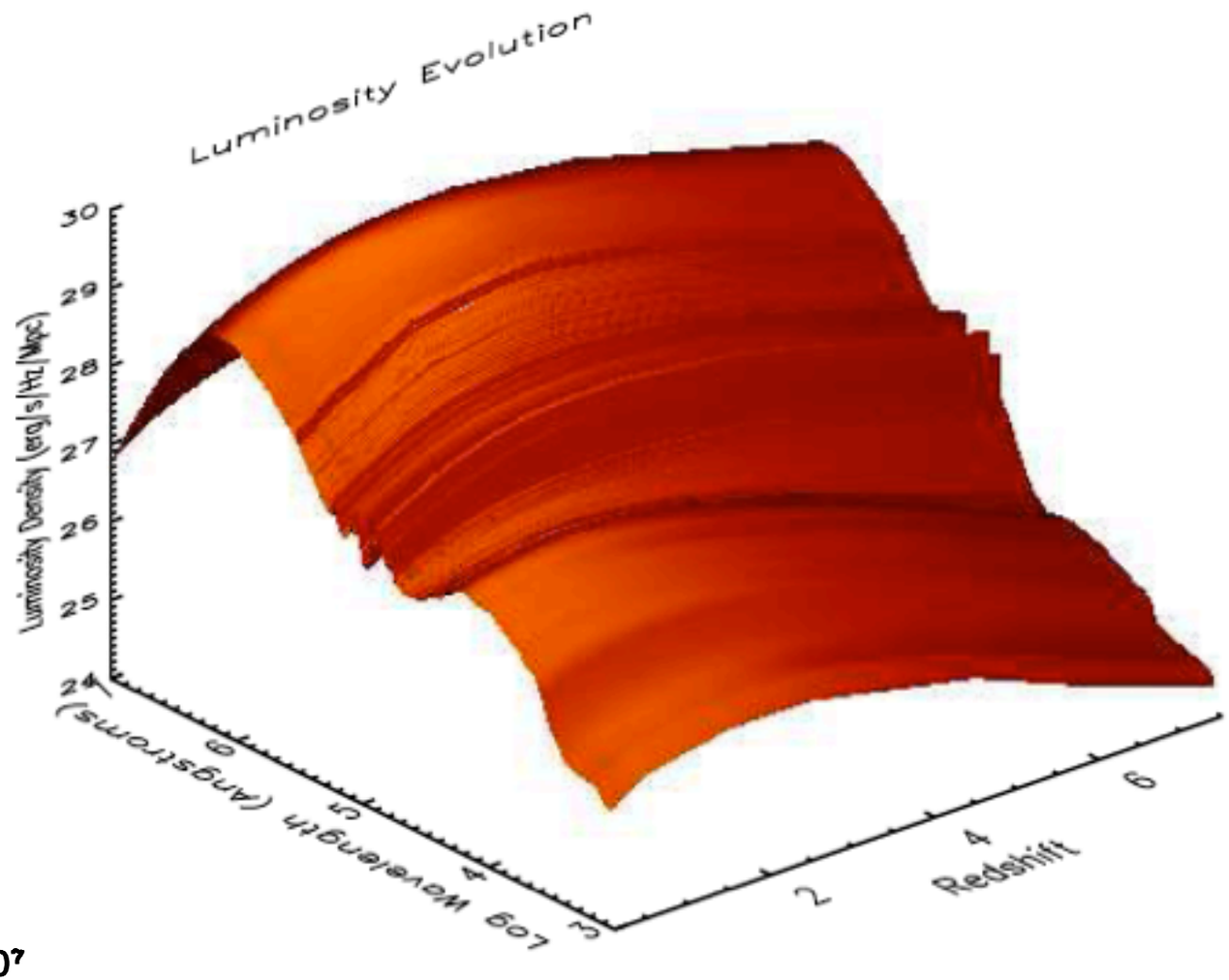

Gilmore, Somerville, Primack, & Dominguez (2012)

Some Results from our Semi-Analytic Models

z=0 Luminosity Functions

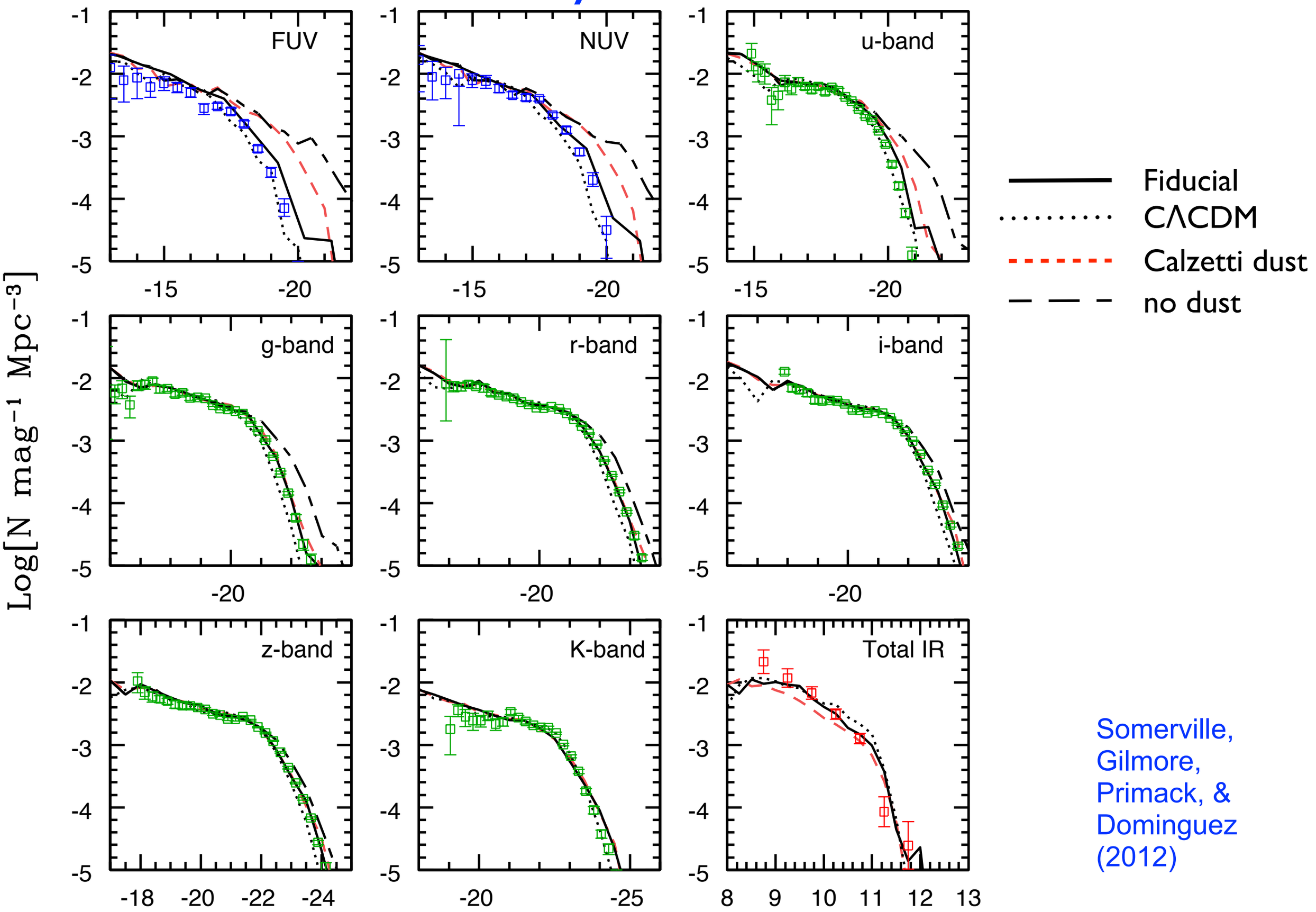

Somerville, Gilmore, Primack, & Dominguez (2012)

Some Results from our Semi-Analytic Models

Number Counts in UV, b, i, z, K Bands

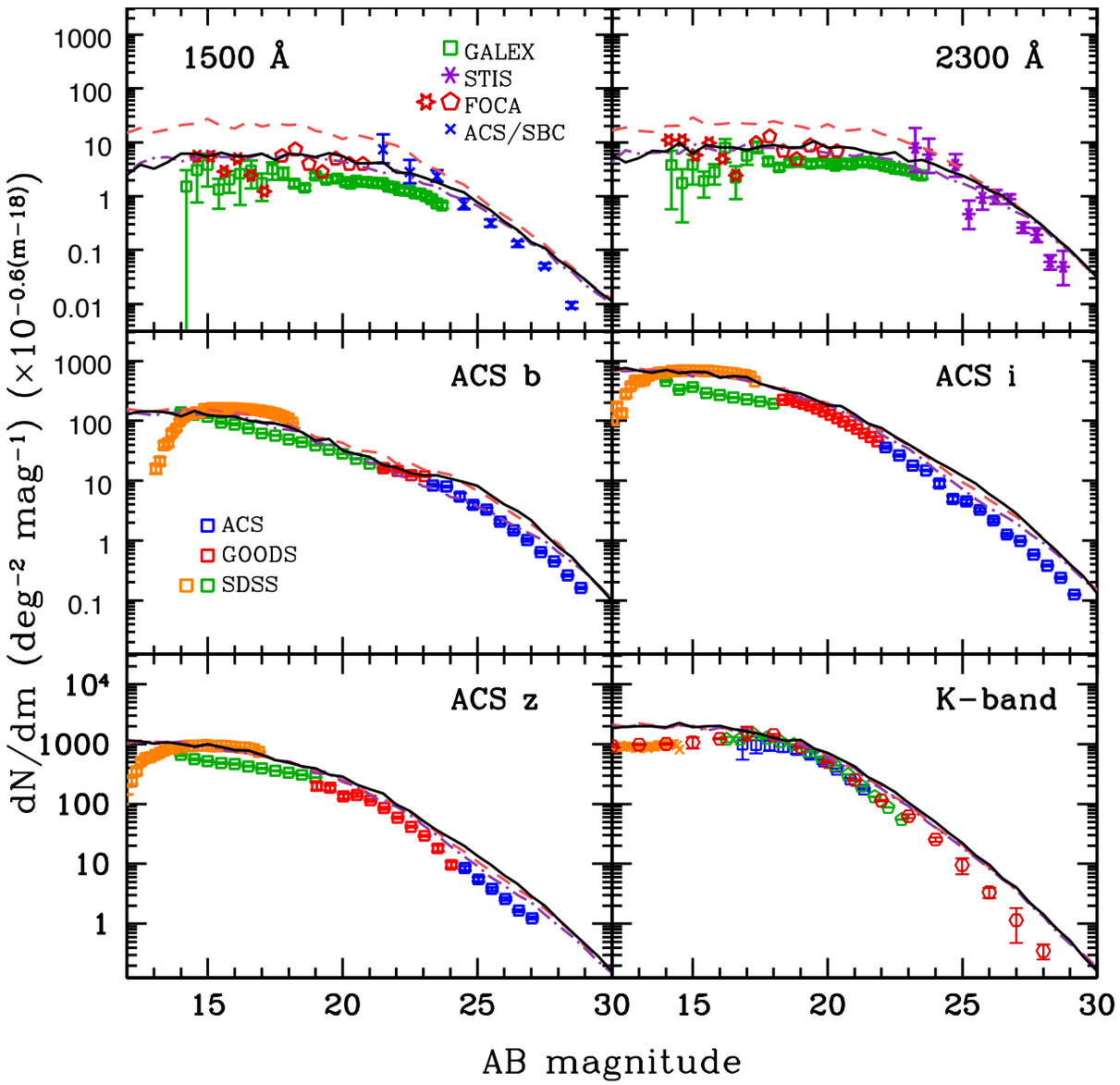

Number Counts in 3.6, 8, 24, 70, 250, & 850 μm Bands

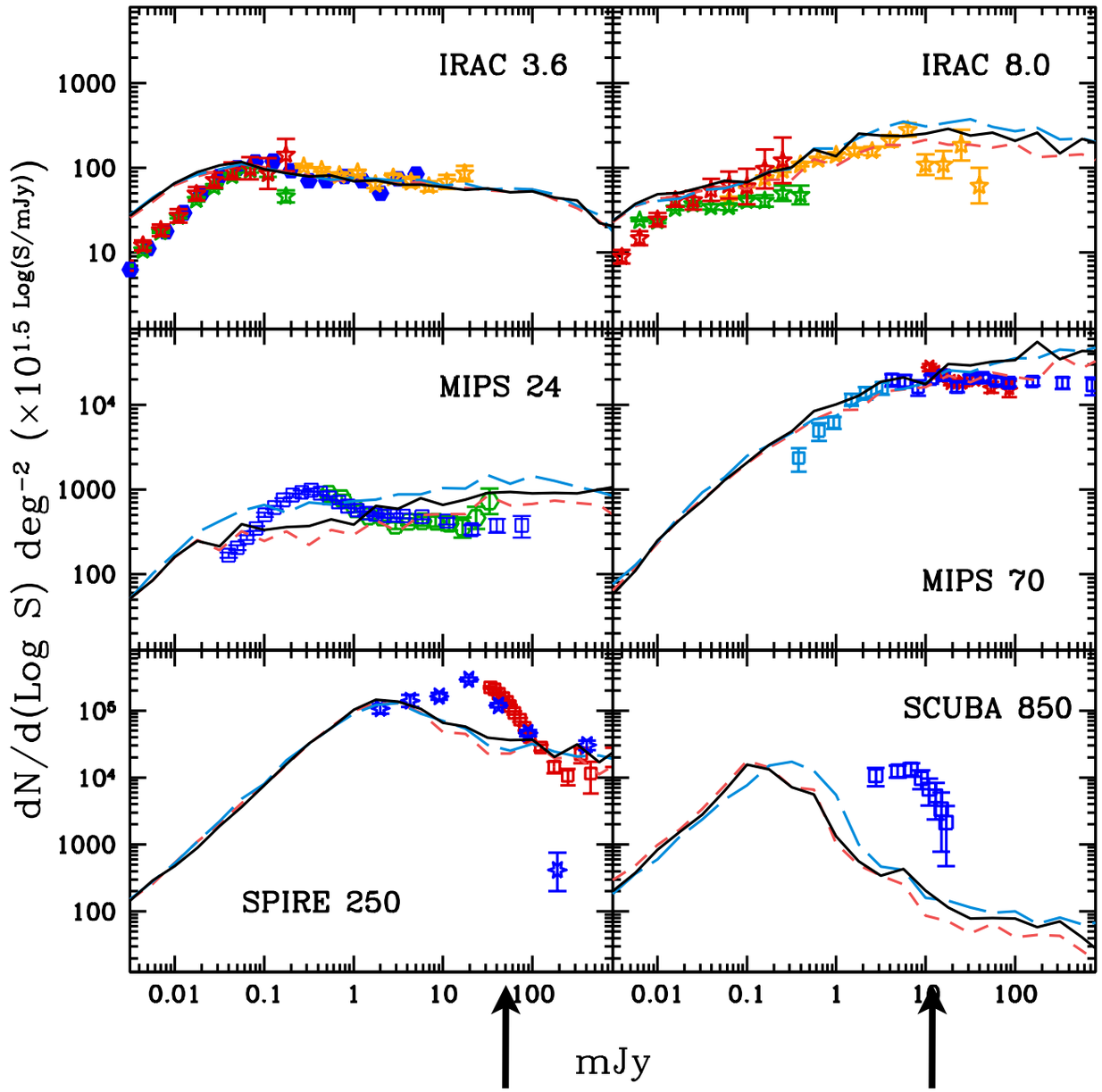

Somerville, Gilmore, Primack, & Dominguez (2012)

Far-IR problems

EBL Observations & Theory

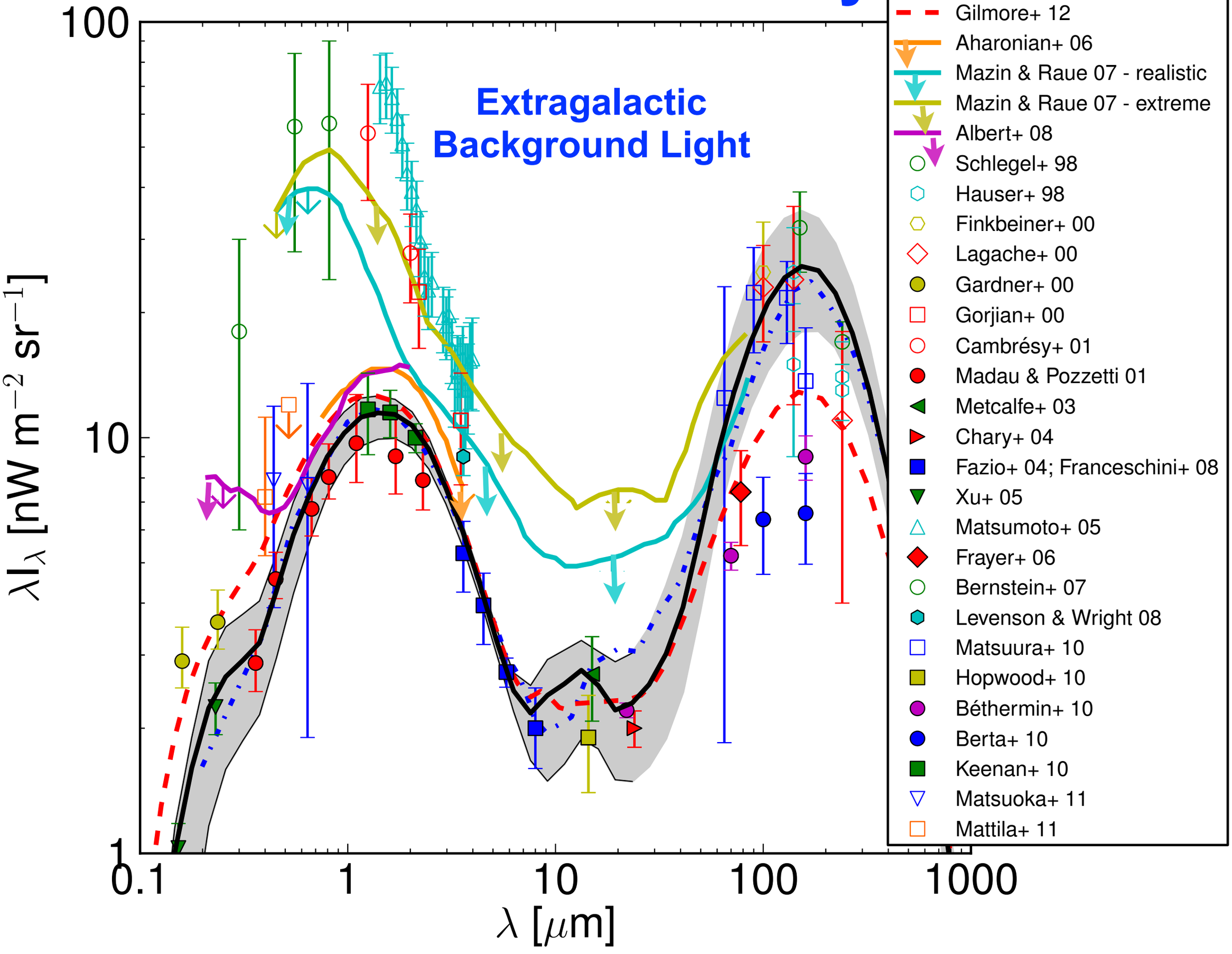

EBL Evolution

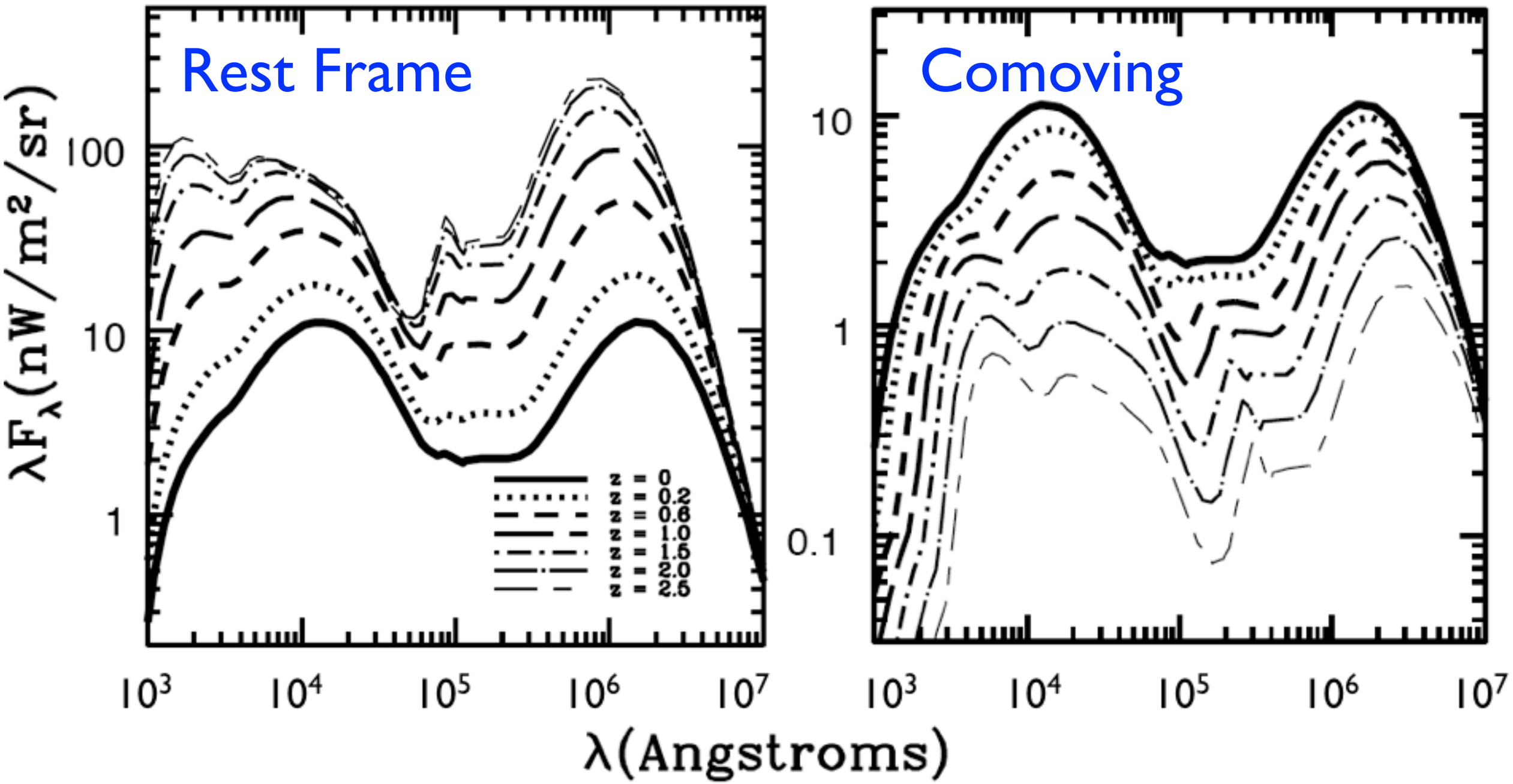

The evolution of the EBL in our WMAP5 Fiducial model. This is plotted on the left panel in standard units. The right panel shows the build-up of the present-day EBL by plotting the same quantities in comoving units. The redshifts from 0 to 2.5 are shown by the different line types in the key in the left panel.

Gilmore, Somerville, Primack, & Dominguez (2012)